Cellular clocks in AVP neurons of the scn are critical for interneuronal coupling regulating circadian behavior rhythm

著者	Mieda Michihiro, Ono Daisuke, Hasegawa Emi, Okamoto Hitoshi, Honma Ken-ichi, Honma Sato, Sakurai Takeshi
journal or publication title	Neuron
volume	85
number	5
page range	1103-1116
year	2015-03-04
URL	http://hdl.handle.net/2297/41375

doi: 10.1016/j.neuron.2015.02.005

Manuscript

Cellular Clocks in AVP Neurons of the SCN Are Critical for Interneuronal Coupling Regulating Circadian Behavior Rhythm

Michihiro Mieda[1], Daisuke Ono[2], Emi Hasegawa[1], Hitoshi Okamoto[3], Ken-ichi Honma[2], Sato Honma[2], Takeshi Sakurai[1]

[1]Department of Molecular Neuroscience and Integrative Physiology, Faculty of Medicine, Kanazawa University, 13-1 Takara-machi, Kanazawa, Ishikawa 920-8640, Japan.

[2]Department of Chronomedicine, Hokkaido University Graduate School of Medicine, N-15, W-7, Kita-ku, Sapporo, Hokkaido 060-8638, Japan.

[3]Laboratory for Developmental Gene Regulation, RIKEN Brain Science Institute, 2-1 Hirosawa, Wako, Saitama 351-0198, Japan.

Corresponding author:

Dr. Michihiro Mieda, Department of Molecular Neuroscience and Integrative Physiology, Faculty of Medicine, Kanazawa University, Kanazawa, Ishikawa 920-8640, Japan; Email: mieda@med.kanazawa-u.ac.jp

Manuscript information: 39 pages, 7 figures, 4 supplemental figures, 1 supplemental table

Numbers of words: Abstract, 147 words; Total, 64,837 characters

SUMMARY

The suprachiasmatic nucleus (SCN), the primary circadian pacemaker in mammals, is a network structure composed of multiple types of neurons. Here, we report that mice with a *Bmal1* deletion specific to arginine vasopressin (AVP)-producing neurons showed marked lengthening in the free-running period and activity time of behavior rhythms. When exposed to an abrupt 8 hr advance of the light/dark cycle, these mice reentrained faster than control mice did. In these mice, the circadian expression of genes involved in intercellular communications, including *Avp*, *Prokineticin 2*, and *Rgs16*, was drastically reduced in the dorsal SCN, where AVP neurons predominate. In slices, dorsal SCN cells showed attenuated PER2::LUC oscillation with highly variable and lengthened periods. Thus, *Bmal1*-dependent oscillators of AVP neurons may modulate the coupling of the SCN network, eventually coupling morning and evening behavioral rhythms, by regulating expression of multiple factors important for the network property of these neurons.

RUNNING TITLE

AVP-neuronal clocks regulate SCN neurons' coupling (50 characters)

INTRODUCTION

The circadian oscillator in the SCN of the hypothalamus is the central pacemaker in mammals, orchestrating multiple circadian biological rhythms in the organism (Reppert and Weaver, 2002). The SCN contains ~20,000 neurons most of which have ability to generate autonomous circadian oscillations. Individual cellular oscillators are driven by autoregulatory transcriptional/post-translational feedback loops (TTFLs) of clock genes in cooperation with cytosolic signaling molecules, such as cAMP and Ca^{2+} (Welsh et al., 2010). Intriguingly, these intracellular processes are not unique to SCN neurons and are common to peripheral cells (Balsalobre et al., 1998). Rather, intercellular communications among SCN clock neurons through the neuronal and diffusible network differentiate the SCN from the peripheral tissues so that it generates highly robust and coherent oscillations at the population level, and these oscillations are strikingly resistant to genetic and environmental perturbations (Welsh et al., 2010).

The SCN is a heterogeneous structure consisting of multiple types of neurons (Antle and Silver, 2005). Most SCN neurons are GABAergic, and several populations of these GABAergic neurons also simultaneously contain neuropeptides. These include AVP-producing neurons located predominantly in the dorsomedial part or the shell of the SCN, as well as vasoactive intestinal peptide (VIP)-producing neurons and gastrin releasing peptide (GRP)-producing neurons, in the ventrolateral part or the core of the SCN. VIP has been demonstrated to be especially important for the maintenance and synchronization of cellular clocks in individual SCN neurons (Aton et al., 2005; Harmar et al., 2002; Maywood et al., 2006). However, other factors, such as GABA, GRP, and AVP, may also play additional roles in the coupling of SCN neurons (Aida et al., 2002; Li et al., 2009; Liu and Reppert, 2000; Maywood et al., 2011; Yamaguchi et al., 2013).

Rhythmic *Per* expression in constant conditions is most prominent in the dorsal SCN, mostly overlapping with the area containing AVP neurons (Hamada et al., 2004). In contrast, the core region contains retinorecipient neurons responding immediately to the photic stimuli and communicating this information to the dorsal SCN (Shigeyoshi et al., 1997; Silver et al., 1996). The SCN core and shell regions send distinct efferent projections to their target areas, primarily in the medial areas of hypothalamus and thalamus (Leak and Moore, 2001).

We considered that neuron type-specific genetic manipulations within the SCN would provide crucial information for understanding the principles underlying the SCN network. In particular, it remains still unknown whether a particular class of neurons functions as the pacemaker to entrain the entire SCN. A study using fully isolated SCN neurons found no evidence for a specialized or anatomically localized class of cell-autonomous pacemakers (Webb et al., 2009). Thus, we decided to take the alternative approach of disrupting cellar oscillators in a neuron type-specific manner and examine the effects on the circadian rhythms of behavior and *Per* expression in the SCN. In this study, we generated mice in which *Bmal1* was deleted specifically in AVP neurons and analyzed circadian rhythms in behavior as well as in SCN cells and tissues. BMAL1 is one of the essential transcription factors of the TTFL and its absence from all SCN neurons has been considered to be sufficient for the extinction of circadian behavioral rhythms in mice (Bunger et al., 2000).

Since AVP-deficient Brattleboro rats display attenuated circadian rhythms but little abnormality in circadian pacemaking, AVP has been considered to serve as an SCN output (Kalsbeek et al., 2010). Therefore, cellular oscillators in AVP neurons may be required for high-amplitude circadian output of the SCN. In addition, recent studies

have implicated AVP in the coupling of SCN neurons (Li et al., 2009; Yamaguchi et al., 2013). Moreover, AVP neurons contain not only AVP but also other neurotransmitters, such as GABA and prokineticin 2 (Prok2) (Antle and Silver, 2005; Masumoto et al., 2006). Multiple transmitters in one neuronal type play differential roles in the neuronal transmission, as exemplified by orexigenic AgRP neurons in the hypothalamic arcuate nucleus (Krashes et al., 2013) and wake-promoting orexin neurons in the perifornical and lateral hypothalamus (Muschamp et al., 2014; Schone et al., 2014). Therefore, we considered it to be important to examine the role of neurons marked by AVP expression in the function of the SCN network.

RESULTS

Generation of *Avp-Cre* Transgenic Mice

To achieve genetic manipulations specifically in AVP neurons, we generated a bacterial artificial chromosome (BAC) transgenic mouse that expressed codon-improved Cre recombinase (Shimshek et al., 2002) under the transcriptional control of *Avp* promoter (*Avp-Cre* mice). To localize Cre activity, *Avp-Cre* mice were crossed with *Rosa26-tdTomato* reporter mice (Ai14 mice), which express tdTomato after Cre-mediated deletion of a *loxP*-flanked transcriptional blocker (Madisen et al., 2010). In these mice, tdTomato expression was mostly restricted in the SCN, supraoptic nucleus (SON), and the paraventricular nucleus (PVH) of the hypothalamus, where many AVP neurons are located (Figures 1 and S1) (Hallbeck et al., 1999). Prominent tdTomato expression was also observed in a significant number of thalamic reticular neurons, where a previous study reported weak *Avp* expression in adult mice and another study suggested its expression in mouse embryos (Visel et al., 2007; Yamaguchi

et al., 2013). In addition to these site, tdTomato expression was detected in some cells scattered in several brain areas, including granule cells of the dentate gyrus, the bed nucleus of the stria terminalis, and the inferior colliculus (Figure S1, also see its legend). Most of this scattered expression was likely to reflect weak expression of *Avp* in the adult and/or developmental expression (Hallbeck et al., 1999; Visel et al., 2007). These data suggested that Cre expression in *Avp-Cre* mice mostly reflects endogenous *Avp* expression with possible ectopic expression in a limited number of cells.

Within the SCN, tdTomato expression was almost completely colocalized with AVP immunoreactivity (99.3% of AVP+ cells were also tdTomato+, 100% of tdTomato+ cells were also AVP+; counts of two SCN slices each from two mice), and there was almost no overlap with VIP immunoreactivity (0.5% of VIP+ cells were also tdTomato+, 0.07% of tdTomato+ cells were also VIP+)(Figure 1A). Thus, Cre-mediated recombination occurred specifically in AVP neurons within the SCN, confirming that *Avp-Cre* mouse is a useful tool for AVP-neuron-specific genetic manipulations to reveal their roles in the central circadian pacemaker of the SCN.

Generation of mice lacking *Bmal1* specifically in AVP neurons (*Avp-Bmal1*$^{-/-}$ mice)

To understand the roles of cellular clocks intrinsic to AVP neurons of the SCN, we next generated mice lacking *Bmal1* specifically in AVP neurons by crossing *Avp-Cre* mice with mice with floxed *Bmal1* alleles (*Bmal1*$^{fl/fl}$) (Storch et al., 2007), hereafter designated *Avp-Bmal1*$^{-/-}$ mice. To quantify the efficiency and specificity of *Bmal1* deletion, *Avp-Bmal1*$^{-/-}$ mice were further crossed to *Rosa26-tdTomato* reporter mice to label AVP neurons with red fluorescent tdTomato. In the SCN of *Avp-Bmal1*$^{-/-}$*;Rosa26-tdTomato* mice, the number of tdTomato+;BMAL1+ neurons

labeled with anti-BMAL1 immunofluorescence was drastically reduced compared with that in control *Avp-Cre;Bmal1*$^{wt/fl}$*;Rosa26-tdTomato* mice (23.0 ± 3.6% and 90.2 ± 2.6% of tdTomato+ cells, respectively, were also BMAL1+, n = 3, $p < 0.001$) (Figure 1B). In contrast, the number of tdTomato-;BMAL1+ cells was not significantly different between the two genotypes (478 ± 74 vs. 602 ± 79 cells/slice, n = 3, $p = 0.316$). Thus, *Bmal1* was deleted efficiently and specifically from AVP neurons in *Avp-Bmal1*$^{-/-}$ mice. Importantly, the number of tdTomato+ cells did not differ between the two genotypes (690 ± 19 vs. 754 ± 22 cells/slice, n = 3, $p = 0.090$), suggesting that AVP neurons remained alive in the absence of BMAL1 expression.

Bmal1 deficiency in AVP neurons lengthens the free-running period and the activity time of circadian behavior rhythm

We next measured the circadian rhythm of spontaneous locomotor activity in *Avp-Bmal1*$^{-/-}$ mice. The behavior of these mice was significantly different from that of control mice (*Bmal1*$^{fl/fl}$ and *Avp-Cre;Bmal1*$^{wt/fl}$ mice; these two behaved similarly, suggesting that Cre expression *per se* did not cause overt abnormality) in 12 hr of light and 12 hr of darkness (LD12:12) (Figures 2A and 2B; Table S1). Nocturnal activities of both groups were bimodal, showing the onset and offset components of activity [or the evening (E) and morning (M) components]. The daily activity profile showed that the activity onset was earlier and the activity time was longer in *Avp-Bmal1*$^{-/-}$ mice compared to control mice (Activity onset, ZT11.24 ± 0.12 vs. ZT11.87 ± 0.05, $p < 0.001$; activity time, 14.16 ± 0.31 hr vs. 12.94 ± 0.22 hr, $p = 0.006$), resulting in more profound drop in the activity level at the middle of the dark phase (Figure 2B). The activity count in the dark phase was significantly reduced in *Avp-Bmal1*$^{-/-}$ mice

compared to control mice (13404 ± 1292 vs. 17536 ± 1352 counts, p = 0.044), while daily total activity counts did not differ significantly (18778 ± 1457 vs. 21410 ± 1479 counts, p = 0.226).

In constant darkness (DD), *Avp-Bmal1*$^{-/-}$ mice showed an activity pattern drastically different from that of control mice (Figures 2A and 2B; Table S1). When released into DD, the activity onset component typically free-ran with shorter periods than the offset component, resulting in a gradual increase of the activity band (*Avp-Bmal1*$^{-/-}$ mice: free-running period of the activity onset, 24.01 ± 0.02 hr; activity offset, 24.59 ± 0.08 hr; control mice: activity onset, 23.90 ± 0.04 hr; activity offset, 24.02 ± 0.03 hr; calculated for days 1–7 in DD). After ca. 2 weeks in DD, the activity onset and offset of the behavior rhythm developed into free-running in parallel, with an identical period approximately 50 min longer than that of control mice (24.80 ± 0.11 hr vs. 23.94 ± 0.03 hr, p < 0.001, days 15–29 in DD). Meanwhile, the activity time reached a steady-state length approximately 5 hr longer than that in controls (19.52 ± 0.47 hr vs. 14.29 ± 0.24 hr, p < 0.001, days 15–29 in DD). In some *Avp-Bmal1*$^{-/-}$ mice, the activity onset gradually became obscure (Figure 2A, middle panel). In addition, the free-running period and activity time fluctuated under prolonged DD in *Avp-Bmal1*$^{-/-}$ mice (Figures 2A and S2). Their phenotype was reminiscent of so-called splitting (Pittendrigh and Daan, 1976). Total daily activity and activity during the activity time were not significantly different between the two groups. In extreme cases, *Avp-Bmal1*$^{-/-}$ mice showed multiple free-running periods and apparent transient arrhythmicity, which was often followed by rhythmic behavior with a lengthened free-running period (observed in 3 out of 21 *Avp-Bmal1*$^{-/-}$ mice crossed to *Per2::Luc* reporter mice, see below)(Figure S2). These results indicate that the cellular circadian oscillation persists, but the mutual

coupling between clock neurons regulating E and M components of activity may be severely impaired in the SCN of *Avp-Bmal1*$^{-/-}$ mice.

Since *Avp* is expressed in several brain regions outside the SCN, as well as in a few peripheral organs during development (Hallbeck et al., 1999; Visel et al., 2007), it is possible that *Bmal1* deletion in the tissues other than the SCN was responsible for the circadian phenotype of *Avp-Bmal1*$^{-/-}$ mice. Furthermore, abnormal circadian rhythm of *Avp-Bmal1*$^{-/-}$ mice could stem secondarily from altered anatomical structure of the SCN network due to the absence of BMAL1 in AVP neurons during development. To address these, we performed restoration experiments. Elongations of the free-running period and the activity time in *Avp-Bmal1*$^{-/-}$ mice were reversed almost completely when *Bmal1* expression was restored in AVP neurons of the SCN using a recombinant adeno-associated virus (AAV) vector, with some off-target restoration (free-running period, 23.84 ± 0.12 hr; activity time, 15.48 ± 0.43 hr) (Figure S2B). This result rules out the peripheral tissues and the developmental defects of the neuronal connectivity of the SCN network as the cause of altered circadian behavior in *Avp-Bmal1*$^{-/-}$ mice. It also suggests that the lack of BMAL1 in AVP neurons of the SCN account for the phenotype of *Avp-Bmal1*$^{-/-}$ mice, given the well-established role of the SCN as the circadian pacemaker.

The sleep/wakefulness cycle of *Avp-Bmal1*$^{-/-}$ mice was almost parallel to their locomotor activity pattern (Figures 2B, C and S2C). In LD12:12, *Avp-Bmal1*$^{-/-}$ mice showed a more profound drop of wakefulness at the middle of the dark phase compared with control mice. Time spent in wakefulness during the dark phase was significantly shorter in *Avp-Bmal1*$^{-/-}$ mice (6.79 ± 0.05 hr vs. 7.89 ± 0.46 hr, $p = 0.032$), whereas total daily wakefulness time did not differ significantly compared with control mice (11.00 ±

0.11 hr vs. 12.16 ± 0.71 hr, p = 0.105). As for sleep/wakefulness in DD, we analyzed EEG/EMG data on days 8–10 in DD, when the activity onset had not substantially deviated from the ZT12 of the preceding LD12:12 in most *Avp-Bmal1*$^{-/-}$ mice (Figure 2A), because it was difficult to precisely determine the onset of the activity time based on EEG/EMG data in mice free-running in DD. The activity time was 4–5 hours longer in *Avp-Bmal1*$^{-/-}$ mice. In addition, the onset of activity time was delayed for approximately an hour in these mice, likely reflecting the lengthening of the free-running period (Figure 2C, right panel). Total daily amounts of wakefulness were not significantly different between the two groups (11.78 ± 0.48 hr vs. 11.78 ± 0.64 hr, p = 0.989). Hourly distributions of non-rapid eye movement (REM) sleep were essentially mirrored by those of wakefulness and paralleled those of REM sleep (Figure S2C). These data suggest that circadian sleep/wakefulness rhythm is altered while homeostatic regulation of sleep/wakefulness remains unchanged in *Avp-Bmal1*$^{-/-}$ mice.

Avp-Bmal1$^{-/-}$ mice show diminished photoperiodic response of behavioral rhythm to the long day-condition and temporal arrhythmicity under DD after long-days

The SCN is composed of thousands of clock neurons, and the phase distribution of these oscillating neurons has been considered to carry information on day length for adaption to seasonal changes (Hazlerigg et al., 2005; Inagaki et al., 2007; Jagota et al., 2000). Therefore, the lengthening of the activity time in *Avp-Bmal1*$^{-/-}$ mice may indicate an impairment of the internal synchronization among SCN neurons in these mice. Thus, we next examined whether these mice can entrain to a long-day, 18 hr light/6 hr dark condition (LD18:6), in which the activity time would be compressed. In LD18:6, *Avp-Bmal1*$^{-/-}$ mice readily shifted their activity onset to the onset of the dark phase, but

the activity offset was significantly phase-delayed in these mice compared to control mice (Time of day: 11.71 ± 0.60 hr vs. 10.28 ± 0.12 hr, p = 0.049), resulting in an elongation of the activity time (12.19 ± 0.54 hr vs. 10.49 ± 0.19 hr, p = 0.019)(Figures 3A and 3B). Intriguingly, when subsequently released into DD from the LD18:6 condition, they exhibited transient arrhythmicity for approximately 1 week, then free-ran with a lengthened period (Figures 3A and 3C). Thus, without the cellular circadian oscillators in AVP neurons, coupling of SCN clock neurons might be unstable in the LD18:6 condition, and this manifested in the removal of zeitgeber when released into DD.

Avp-Bmal1$^{-/-}$ mice reentrain faster than control mice upon a phase shift of the LD cycle

To further elucidate the state of internal coupling among SCN neurons, we examined the behavior of _Avp-Bmal1_$^{-/-}$ mice during the sudden shifts of an LD cycle. Upon a 4-hr phase shift of the LD cycle, both _Avp-Bmal1_$^{-/-}$ mice and control mice demonstrated a gradual shift of locomotor activity rhythms to reentrain to the new LD cycle (Figure 4A). Nevertheless, the number of days required for full reentrainment was significantly shorter in _Avp-Bmal1_$^{-/-}$ mice compared to control mice when LD cycle was advanced by 4 hr (5.86 ± 0.13 days vs. 6.88 ± 0.40 days, p = 0.031) (Figure 4B). In contrast, upon an 8-hr phase advance, _Avp-Bmal1_$^{-/-}$ mice did not show the gradual shift of locomotor activity during the reentrainment demonstrated by control mice; the onset and offset components of activity shifted in parallel (Figure 4C). Instead, these components did not show coordinated shifting during the reentrainment period and were segregated in multiple components with different periods. Indeed, periodogram analysis demonstrated

that the peak of the periods within the circadian range was drastically attenuated to nearly non-significant levels during the reentrainment in *Avp-Bmal1*$^{-/-}$ mice (Figure 4E). Subsequently, these mice were entrained to the new LD cycle in about a week. The number of days required for reentrainment was significantly fewer in *Avp-Bmal1*$^{-/-}$ mice compared to control mice for 8-h phase shifts of both advance and delay (phase advance: 8.50 ± 0.73 days vs. 13.71 ± 1.36 days, $p = 0.004$; phase delay: 4.50 ± 0.29 days vs. 6.67 ± 0.67 days, $p = 0.021$) (Figure 4D). These results are consistent with the idea that interneuronal coupling among SCN neurons is weakened in *Avp-Bmal1*$^{-/-}$ mice.

Light-responsiveness of the SCN and behavior rhythm is altered in *Avp-Bmal1*$^{-/-}$ mice

We next examined the light-responsiveness of *Avp-Bmal1*$^{-/-}$ mice by measuring the phase-shift of activity rhythms evoked by light pulses. Because *Avp-Bmal1*$^{-/-}$ mice often showed ambiguous onset of activity in DD (Figures 2A and S2), we applied the Aschoff Type II method to examine phase responses of behavior rhythms (Aschoff, 1965), by applying a 30-min light pulse at ZT14 and then housing mice in DD. The phase-delaying effects of these light pulses were significantly attenuated in *Avp-Bmal1*$^{-/-}$ mice compared to control mice (0.39 ± 0.16 hr vs. 1.32 ± 0.13 hr, $p < 0.001$) (Figures 5A and 5B). It should be noted that even the Aschoff Type II method might not allow us to precisely measure the light-responsiveness of *Avp-Bmal1*$^{-/-}$ mice, because the activity onset changes the free-running period after approximately a week in DD. Nevertheless, the induction of *Per1* mRNA expression in the core of the SCN by the same light pulses was also reduced in *Avp-Bmal1*$^{-/-}$ mice compared with control mice at ZT15 ($p = 0.005$) (Figures 5C and 5D).

Thus, the absence of *Bmal1* in AVP neurons may reduce the responsiveness of the ventral SCN to light. Alternatively, the shape of the phase-response curve (PRC) might be changed in *Avp-Bmal1*$^{-/-}$ mice, due to the decompression of their activity band, such that responses to light pulses at ZT14 were attenuated. Importantly, AVP neurons do not directly respond to the signals conveyed through the retinohypothalamic tract (Antle and Silver, 2005). Instead, light-responsive cells are located in the ventral SCN, which does not contain AVP neurons. One possible explanation for this discrepancy is that timing information from AVP neurons may modulate the sensitivity of light-responsive cells to the light, according to a previous report of the reciprocal interaction between the dorsal and ventral SCN (Albus et al., 2005). Moreover, the weaker light-responsiveness of *Avp-Bmal1*$^{-/-}$ mice apparently contradicts their faster reentrainment upon a phase shift of the LD cycle (Figure 4). This can be explained as follows: Although acute response to a brief light pulse is attenuated, repetitive exposure to light stimuli entrains the SCN of *Avp-Bmal1*$^{-/-}$ mice more efficiently due to the weakened interneuronal coupling among SCN neurons.

Changes in gene expression in the SCN of *Avp-Bmal1*$^{-/-}$ mice

We next examined the effects of *Bmal1* deficiency in AVP neurons on the circadian expression of genes that play important roles in the SCN network (Figures 6 and S3). In *Avp-Bmal1*$^{-/-}$ mice, mRNA expression of *Per1*, one of the core components of circadian clocks, was attenuated specifically in the dorsal part of the SCN, where most AVP neurons are located, compared with control mice. In addition, *Avp* mRNA and peptide expression was drastically attenuated in the SCN of *Avp-Bmal1*$^{-/-}$ mice. Intriguingly, *Avp* expression in other nuclei, such as the PVH and SON, remained unchanged (Figure S3),

suggesting that transcriptional regulation of *Avp* by CLOCK:BMAL1 is a feature unique to SCN neurons. These results are consistent with the finding that *Avp* mRNA and peptide levels were reduced in the SCN, but not in the SON, of *Clock/Clock* mice (Jin et al., 1999).

Furthermore, mRNA expression of *Prokineticin 2* (*Prok2*), a peptide considered an output signaling molecule of the SCN (Cheng et al., 2002; Masumoto et al., 2006), as well as of *Rgs16* (*regulator of G protein signaling 16*)(Doi et al., 2011), was markedly decreased specifically in the dorsal part of the SCN in *Avp-Bmal1*$^{-/-}$ mice compared with control mice, suggesting that expression levels of these genes were substantially reduced in AVP neurons but remained relatively normal in non-AVP neurons. In clear contrast, *Vip* mRNA expression in these mice was comparable to control mice. These data suggest that cellular oscillators in AVP neurons coordinate the circadian expression of multiple factors involved in intercellular and intracellular pathways of these neurons.

Cells in the dorsal SCN of *Avp-Bmal1*$^{-/-}$ mice oscillate with low amplitudes and variable periods in culture

To investigate the impacts of *Bmal1* deletion in AVP neurons on the action of the SCN cellular network, we performed real-time bioluminescence monitoring of SCN slices prepared from control and *Avp-Bmal1*$^{-/-}$ mice expressing a luciferase reporter (PER2::LUC)(Yoo et al., 2004). Compared with control mice, SCN slices from *Avp-Bmal1*$^{-/-}$ mice housed in DD for more than 3 weeks showed attenuated and noisy wave forms of PER2::LUC luminescence, which dampened within 5–6 cycles in most mice (the first peak counts of detrended waves: 994 ± 218 vs. 2356 ± 307 counts/min, $p = 0.001$) (Figure 7A). The mean period of the first 3 cycles in culture was significantly

longer in *Avp-Bmal1*$^{-/-}$ mice (24.34 ± 0.18 hr vs. 23.91 ± 0.06 hr, p = 0.036) (Figure 7B). However, the extent of lengthening was tiny compared with that observed for the behavioral free-running period described above (Figure 2). Notably, elongation of the period of PER2::LUC oscillation in *Avp-Bmal1*$^{-/-}$ mice was larger for the first cycle (25.02 ± 0.36 hr vs. 23.94 ± 0.10 hr, p = 0.010), which was comparable to the behavioral free-running period, but it disappeared in the second cycle (23.82 ± 0.29 hr vs. 23.97 ± 0.09 hr, p = 0.632) (Figure 7B). Thus, the period of SCN oscillation in vivo may not be maintained in culture for a long duration.

To further elucidate the impairment of the SCN network of *Avp-Bmal1*$^{-/-}$ mice, PER2::LUC expression was measured at cellular resolution by bioluminescent cell imaging in the middle SCN along the rostro-caudal axis, which contains both the shell and core regions. Because the traditional ROI method appeared to be difficult to apply to the dorsal SCN of *Avp-Bmal1*$^{-/-}$ mice due to its drastic attenuation of PER2::LUC oscillation, we conducted pixel-based analyses. Thus, for the PER2::LUC oscillations in the individual pixels covering the SCN, we performed cosine curve fittings and calculated the amplitude and period for the data from 25–72 hr after slice preparations (Figures 7C and S4A). The resolution of images was adjusted to 4.3 μm/pixel. In *Avp-Bmal1*$^{-/-}$ mice, as expected, the amplitudes of PER2::LUC oscillation were substantially decreased in the dorsal part of the SCN, where AVP neurons predominate (Figures 7C and 7D). Nevertheless, most of the pixels in the dorsal region demonstrated statistically significant circadian oscillation of PER2::LUC expression, although these oscillations were sloppier compared with those in control mice, as indicated by the considerable reduction in the percent rhythm (PR; percentage of overall variance attributed to the best fitted cosine curve) (Figure S4B). Notably, pixels in the dorsal

SCN of *Avp-Bmal1*$^{-/-}$ mice showed significantly broader distributions of periods compared with those in the ventral SCN or to those in the control mice, suggesting that the variability of periods of the individual pixels' oscillations was strikingly increased in the dorsal SCN of *Avp-Bmal1*$^{-/-}$ mice (mean SD of period in the dorsal SCN: 3.28 ± 0.42 hr vs. 1.19 ± 0.21 hr, p = 0.001) (Figures 7E and 7G). Intriguingly, the mean period of the individual pixels' oscillations in the dorsal SCN was significantly longer in *Avp-Bmal1*$^{-/-}$ mice (26.83 ± 0.86 hr vs. 24.13 ± 0.30 hr, p = 0.018) (Figures 7E and 7F), and it was not significantly different from the behavioral free-running period immediately preceding slice preparations (*Avp-Bmal1*$^{-/-}$*;Per2::Luc* mice, 25.41 ± 0.26 hr, p = 0.191 vs. PER2::LUC oscillation in the dorsal SCN; *Control;Per2::Luc* mice, 23.89 ± 0.05 hr, p = 0.444). These parameters in the ventral SCN did not differ significantly between control and *Avp-Bmal1*$^{-/-}$ mice. When the same calculations were performed on the data for 49–96 hr after slice preparations, such an elongation of the mean period of cellular PER2::LUC oscillations in the dorsal SCN was decreased compared with the value for the data for 25–72 hr, and it did not reach statistical significance (24.00 ± 0.22 hr vs. 23.21 ± 0.31 hr, p = 0.059) (Figures 7F and S4A). Such a temporal change of the period was consistent with the observation in the whole-SCN analyses described above (Figure 7B), suggesting that the lengthening of the period of PER2::LUC oscillation in the SCN of *Avp-Bmal1*$^{-/-}$ mice may not continue stably in slices. In contrast, the increase in the variability of period in the dorsal SCN of these mice persisted in the data for 49–96 hr (mean SD of period: 3.30 ± 0.28 hr vs. 1.37 ± 0.24 hr, p < 0.001) (Figure 7G). Importantly, the differences between the two periods of individual pixels calculated for different time windows (25–72 hr or 49–96 hr) were strikingly increased in the dorsal SCN of *Avp-Bmal1*$^{-/-}$ mice compared with control mice (5.46 ± 0.83 vs. 1.95 ± 0.24 hr, p

= 0.003), suggesting that there is considerable fluctuation of individual pixels' oscillations.

Collectively, these results suggest that cells in the dorsal SCN of *Avp-Bmal1*$^{-/-}$ mice oscillate with low amplitudes and with highly variable and unstable periods. As an ensemble, the dorsal SCN of these mice may oscillate with a lengthened period.

DISCUSSION

Disruption of cellular oscillators restricted to AVP neurons alters the behavioral free-running period

In this study, we demonstrated that *Bmal1* deletion in AVP neurons lengthens the free-running period and the activity time of behavior rhythm. Several mouse mutants, including *Clock*$^{\Delta 19}$, *Cry1*$^{-/-}$, *Cry2*$^{-/-}$, *After-hour* (*Afh*)/*Overtime* (*Ovtm*), and *CK1ε*^{tau}, have been reported to free-run with longer or shorter periods (Godinho et al., 2007; Lowrey and Takahashi, 2004; Meng et al., 2008; Siepka et al., 2007). In these mice, all SCN neurons are impaired uniformly due to mutations of clock genes. In clear contrast, cellular clocks in non-AVP neurons are believed to remain intact in *Avp-Bmal1*$^{-/-}$ mice. Nevertheless, these mice show longer free-running period. To our knowledge, the current study reports the first characterization of mice in which circadian cellular oscillators are disrupted only in a distinct neuronal population of the SCN with a specific neurotransmitter identity. It should be noted that ~20% of SCN AVP neurons in *Avp-Bmal1*$^{-/-}$ mice retained at least one intact allele of *Bmal1*, allowing the possibility that complete *Bmal1* deletion in AVP neurons would cause more profound abnormality in the function of the SCN network and in circadian rhythms.

A previous study of wildtype-*Clock*$^{\Delta 19/\Delta 19}$ mutant chimera analysis demonstrated

that circadian behavior in chimeric individuals was determined by the proportion of mutant versus normal cells, and that a number of intermediate phenotypes were seen in balanced chimeras (Low-Zeddies and Takahashi, 2001). In the SCN of these chimeric mice, in other words, random subsets of wildtype SCN cells were replaced with *Clock*$^{\Delta 19/\Delta 19}$ cells. In *Avp-Bmal1*$^{-/-}$ mice; by contrast, a defined subset of SCN neurons (i.e., AVP neurons) was replaced with *Bmal1*$^{-/-}$ neurons. They expressed a novel circadian phenotype that was not intermediate between those of wildtype and *Bmal1*$^{-/-}$ mice, suggesting an AVP neuron-specific role in the SCN pacemaking. Interestingly, continuous activation of Gq-dependent pathways specifically in VIP neurons lengthened the period and decreased the amplitude, and further reprogramed the spatiotemporal dynamics of PER2::LUC rhythm across the entire SCN in slices (Brancaccio et al., 2013). Thus, various neuronal type-specific manipulations of cellular clocks would provide further clues to understanding the principle of the SCN network.

BMAL1-driven cellular oscillators coordinate the expression of multiple factors involved in intercellular communications in AVP neurons

We found profound reductions in the expression of *Avp*, *Prok2*, and *Rgs16* in the dorsal SCN of *Avp-Bmal1*$^{-/-}$ mice. This result is consistent with the fact that promoter regions of these genes contain E-box elements, which are critical for CLOCK-BMAL1-mediated transcriptional activation (Cheng et al., 2002; Doi et al., 2011; Jin et al., 1999). Reportedly, mice lacking the V1a receptor, the principal receptor for AVP in the SCN, demonstrate significant elongation of the activity time in DD, by approximately 100 minutes (Li et al., 2009). Another study reported that *V1a*$^{-/-}$*;V1b*$^{-/-}$ mice immediately reentrain to phase-shifted LD cycles, whereas their free-running

rhythms remain normal, suggesting that AVP-mediated interneuronal communication confers on the SCN an intrinsic resistance to external perturbations such as jet lag (Yamaguchi et al., 2013). Thus, there is a partial overlap of phenotype between these mice and *Avp-Bmal1*$^{-/-}$ mice.

Prok2 is a peptide expressed in subpopulations of AVP, VIP, GRP, and other types of neurons in the SCN (Masumoto et al., 2006). *Prok2*$^{-/-}$ mice also partially share the phenotype of *Avp-Bmal1*$^{-/-}$ mice (Li et al., 2006). They free-run with a period approximately 50 min longer than that of wildtype mice in the C57BL/6 background. In addition, the representative actograms suggested that they have a slightly lengthened activity time. To date, AVP and Prok2 have been considered output signaling molecules of the SCN (Cheng et al., 2002; Jin et al., 1999; Kalsbeek et al., 2010). Nevertheless, receptors for these secreted molecules are expressed in the SCN, and neurons expressing these peptides form a local circuit within the SCN (Castel et al., 1990; Cheng et al., 2002; Li et al., 2009; Masumoto et al., 2006; Yamaguchi et al., 2013). Therefore, the AVP and Prok2 signaling pathways may play indispensable roles in the interneuronal coupling of the SCN network.

Finally, *Rgs16*$^{-/-}$ mice have been reported to free-run with a period approximately 30 min longer than wildtype mice (Doi et al., 2011). Rgs16 inactivates Gi signaling by enhancing GTP hydrolysis, resulting in the increase of cAMP production. The authors concluded that the loss of temporally precise regulation of the cAMP signal by RGS16 leads to an abnormal phase relationship between the dorsomedial and ventrolateral SCN, and this underlies the elongation of free-running period in *Rgs16*$^{-/-}$ mice. Notably, VIP receptor 2 is Gs-coupled, raising the possibility that expression of RGS16 may enhance VIP signaling to coordinate the intercellular

synchrony of SCN pacemaker neurons (Aton et al., 2005; Doi et al., 2011), which, however, is extremely suppressed in the dorsal SCN of *Avp-Bmal1*$^{-/-}$ mice.

Because we saw drastic attenuations of *Avp*, *Prok2*, and *Rgs16* expression in the dorsal SCN of *Avp-Bmal1*$^{-/-}$ mice, their phenotype may be interpreted as the summation of the phenotypes of mice lacking any one of these signaling pathways. It should be emphasized that the phenotype of *Avp-Bmal1*$^{-/-}$ mice is not solely ascribed to the loss of AVP expression, considering the normal free-running periods of behavior in *V1a*$^{-/-}$*;V1b*$^{-/-}$ mice and AVP-deficient Brattleboro rats (Kalsbeek et al., 2010; Yamaguchi et al., 2013). Multiple transmitters other than AVP are also expressed in AVP neurons, including Prok2, GABA, and possibly unidentified factors, which may function in concert and contribute differentially to mediating the output of cellular oscillators in AVP neurons for the proper coupling of SCN neurons.

The fact that *Bmal1*-deficiency caused attenuated expression of factors involved in intercellular communications raises an important question: Which is responsible for the phenotype of *Avp-Bmal1*$^{-/-}$ mice, the attenuation of intercellular communication or the disruption of the molecular oscillation? However, cellular coupling is known to reinforce cellular rhythms (Maywood et al., 2006; Webb et al., 2009), suggesting the reciprocal regulation between the molecular clock and intercellular communications. Therefore, it seems difficult to differentiate between these two possibilities.

BMAL1-driven cellular oscillators in AVP neurons enhance and stabilize circadian oscillation of the SCN network

Although their amplitudes and robustness were drastically attenuated, most cells (pixels) in the dorsal SCN of *Avp-Bmal1*$^{-/-}$ mice demonstrated significant oscillation of

PER2::LUC expression in vitro. This region appeared to contain AVP neurons lacking *Bmal1*, as well as non-AVP neurons and a small number of AVP neurons sustaining an undeleted *Bmal1* allele. PER2::LUC oscillations in *Bmal1*–deleted AVP neurons were most likely driven by cytosolic signaling (Welsh et al., 2010) stimulated by oscillatory inputs from non-AVP neurons in the ventral SCN, where PER2::LUC oscillation was relatively normal. *Bmal2* in AVP neurons, a paralog of *Bmal1* expressed at low level in the SCN, might also contribute (Ko et al., 2010). However, the variability of cellular periods was strikingly larger in the dorsal SCN of *Avp-Bmal1*$^{-/-}$ mice. Consequently, the mean period in the dorsal SCN was lengthened.

These observations are at least partially consistent with the previous report of *Bmal1*$^{-/-}$ mice (Ko et al., 2010). In the SCN slices from *Bmal1*$^{-/-}$ mice, inter-peak intervals of cellular oscillations were variable. However, their average period was shorter than that of wildtype mice. Notably, simulation studies in the same report suggested that the average period would be lengthened when the variation in biochemical parameters increases. Therefore, it is tempting to speculate that such a condition may be occurring in the dorsal SCN of *Avp-Bmal1*$^{-/-}$ mice.

A majority of efferent projections from the SCN to the extra-SCN regions originates in the shell of SCN (Leak and Moore, 2001), including those to the dorsomedial hypothalamic nucleus and to the subparaventricular zone, which are reportedly critical for the circadian rhythms of locomotor activity and sleep/wakefulness (Chou et al., 2003; Lu et al., 2001). Thus, impairments of cellular circadian oscillations in the dorsal SCN might have a profound influence on the SCN output to behavioral rhythms in *Avp-Bmal1*$^{-/-}$ mice.

In slice cultures of *Avp-Bmal1*$^{-/-}$ mice, dorsal SCN oscillated with a mean period

longer than that of ventral SCN. To generate a coherent rhythm in vivo, the dorsal and ventral SCN should be synchronized. Thus, as a result of reciprocal interaction, the SCN of *Avp-Bmal1*$^{-/-}$ mice may send out a rhythmic signal with a period intermediate between those of the dorsal and ventral SCN to drive locomotor activity. Indeed, in cultures from *Avp-Bmal1*$^{-/-}$ mice, the ventral SCN contained a small population of cells oscillating with lengthened periods for ~72 hr in culture, and this may be a signature of such an interaction expected in vivo (Figures 7E). Alternatively, these cells are merely reflecting a small number of AVP neurons located in the ventral portion of the SCN.

The fact that we failed to simply reproduce the lengthening of behavioral free-running period in the PER2::LUC oscillation of prolonged SCN cultures suggests that the intact structure of the SCN and/or its connections with the extra-SCN regions may be indispensable in the establishment of the behavioral free-running period by modulating and stabilizing the properties of the SCN network. In prolonged culture, newly formed networks involving intact non-AVP neurons may compensate the impaired rhythms of AVP neurons lacking *Bmal1*. Inconsistencies between the behavioral free-running period and the period of *Per1-Luc*, *Per1-Gfp*, or PER2::LUC oscillations in the SCN slices have been also reported by previous studies (Aton et al., 2004; Hughes et al., 2008; Mickman et al., 2008; Molyneux et al., 2008).

Morning and evening oscillators in *Avp-Bmal1*$^{-/-}$ mice

The dual oscillator model was originally developed to account for several circadian properties of nocturnal rodents, including bimodal activity patterns and the ability to measure seasonal changes of day length (Pittendrigh and Daan, 1976). This model assumes two separate circadian oscillators, i.e., morning (M) and evening (E) oscillators,

that drive morning and evening activities, respectively. M and E oscillators are normally coupled to maintain the constant length of the activity time.

In *Drosophila*, M and E peaks of activity are differently controlled by the PDF-positive small ventral lateral neurons (s-LN_v) and PDF-negative dorsal lateral neurons (LN_d) (plus at least fifth s-LN_v), respectively (Grima et al., 2004; Helfrich-Forster, 2009; Stoleru et al., 2004). Also in the SCN, separate oscillating cell groups phase-locked to either of the M and E components of locomotor activity have been reported, and M and E oscillators may be located in the rostrocaudal plane of the SCN (Hazlerigg et al., 2005; Inagaki et al., 2007; Jagota et al., 2000). However, there are no reports of defined areas of the SCN that contain exclusively M or E oscillators. Therefore, distributed networks of M and E cells may function as M and E oscillators, respectively. Alternatively, since there are many other clock neurons that oscillate with widely differing phases that cannot be clearly identified as M or E neurons, the distribution of phases of clock neurons, rather than simply two oscillators, may determine the onset and offset of activity time (Helfrich-Forster, 2009). In either case, weakened coupling between mechanisms driving M and E components (or M and E oscillators) may explain the phenotype of *Avp-Bmal1*$^{-/-}$ mice. Given the alterations of both M and E components in *Avp-Bmal1*$^{-/-}$ mice, we further speculate that both mechanisms (oscillators) reside in the network of AVP neurons, of which the phase relationship is further regulated by non-AVP neurons including those releasing VIP.

A model for how cellular oscillators in AVP neurons regulate the coupling of the SCN network

In summary, we propose the following model. Circadian clocks in AVP neurons control

the expression of multiple factors important for interneuronal communications, including secreted factors such as AVP and Prok2, and factors such as RGS16 that regulate the sensitivity of AVP neurons to extracellular signaling molecules such as VIP. In *Avp-Bmal1*$^{-/-}$ mice, the dorsal SCN cells oscillate less robustly with attenuated amplitudes. They may include AVP neurons that lack their intrinsic clocks but continue to oscillate driven by circadian signals from non-AVP neurons. However, due to the reduction in transmitters such as AVP and Prok2, coupling among AVP neurons is attenuated. In addition, diminished Rgs16 expression may reduce the responsiveness of these cells to synchronizers such as VIP, resulting in further weakening of interneuronal coupling. These defects may collectively make the cellular oscillation of AVP neurons highly variable and unstable, and it is lengthened on average. Such changes in the properties at the cellular and network levels manifest at behavior level as the lengthening of the free-running period and activity time, which often fluctuate, as multiple free-running periods, and as transient arrhythmicities upon sudden changes of lighting conditions.

Finally, our results suggest that AVP neurons are involved in the pacemaking function of the SCN network, likely through interactions with other types of SCN neurons, to generate precise circadian rhythmicity.

ACKNOWLEDGEMENTS

This study was supported in part by Grants-in-Aid for Scientific Research (B) (20390056, 24390052) and for Scientific Research on Innovative Areas (25126708) from JSPS and MEXT of Japan; by Career Development Award from the HFSP; by the Takeda Science Foundation (M.M.); by the Cabinet Office, Government of Japan

through its “Funding Program for Next Generation World-Leading Researchers” (LS048) (T.S.); and by the JSPS Research Fellowship for Young Scientists (E.H.). We thank N. G. Copeland for recombineering reagents; R. Sprengel for *iCre* cDNA; J. Takeda for *p23loxZeo*; K. Deisseroth for *pAAV-DIO-hChR2(H134R)-EYFP-WPRE-pA*; B. Roth for *pAAV-DIO-mCherry*; I. Schmutz for *Bmal1 ext* promoter; K. Yagita for *Bmal1* cDNA; Penn Vector Core for *pAAV2-rh10*; C. J. Weitz for the *Bmal1*$^{fl/f}$ mouse; and J. Takahashi for the *Per2::Luc* reporter mouse. We thank H. Nakanishi for technical assistance.

EXPERIMENTAL PROCEDURES

All experimental procedures involving animals were approved by the appropriate institutional animal care and use committees of Kanazawa University, Hokkaido University, and RIKEN BSI. See also Supplemental Experimental Procedures.

Generation of *Avp-Bmal1*$^{-/-}$ Mice

For generating *Avp-Cre* mice, a BAC clone (RP23-100C5), which contains genomic DNA derived from C57BL/6J encompassing the *Avp* gene, was modified to insert the improved Cre recombinase immediately 5' to the translation initiation codon of *Avp* gene. The circular modified BAC was microinjected into fertilized mouse eggs (C57BL/6J strain) to generate founder lines.

Behavioral Analyses

Spontaneous locomotor activity was monitored by infrared motion sensors. Analyses of recorded data were carried out using ClockLab (Actimetrics).

Histological Study

Immunostaining and in situ hybridization were performed as previously described (Hasegawa et al., 2014; Mieda et al., 2006). To examine the specificity of Cre-mediated recombination, *Avp-Cre*;*Rosa26-tdTomato* mice were pretreated with intracerebroventricular injections of colchicine (40 μg in 1 μl saline) for 48 h before transcardial perfusion of 4% paraformaldehyde fixative.

Bioluminescence Imaging

Avp-Bmal1$^{-/-}$ mice were further mated with *Per2::Luc* reporter mice (Yoo et al., 2004). Mice were housed in DD for 3 to 10 weeks before sampling. PER2::LUC bioluminescence at the SCN tissue level was measured from coronal slices of 300 μm with a photomultiplier tube (Kronos Dio). PER2::LUC bioluminescence at the single SCN cell level was measured from coronal slices of 100 μm with an EMCCD camera. Data for the individual pixels were detrended and cosine curve-fitted using a custom-made program.

Statistical Analysis

All results are expressed as mean ± SEM. For comparisons of two groups of normally distributed data, Student's t-tests were performed. For Figures 6B and 7D-G, data from every combination of two groups were analyzed by two-way repeated-measures ANOVA. For comparison of three groups in Figure S2B and Table S1, one-way repeated-measures ANOVA followed by Tukey-HSD *post hoc* tests were performed. Probability (p) values less than 0.05 were considered to be statistically significant. Only relevant information from the statistical analysis is indicated in the text, figures, and table.

REFRENCES

Aida, R., Moriya, T., Araki, M., Akiyama, M., Wada, K., Wada, E., and Shibata, S. (2002). Gastrin-releasing peptide mediates photic entrainable signals to dorsal subsets of suprachiasmatic nucleus via induction of Period gene in mice. Mol Pharmacol *61*, 26-34.

Albus, H., Vansteensel, M.J., Michel, S., Block, G.D., and Meijer, J.H. (2005). A GABAergic mechanism is necessary for coupling dissociable ventral and dorsal regional oscillators within the circadian clock. Curr Biol *15*, 886-893.

Antle, M.C., and Silver, R. (2005). Orchestrating time: arrangements of the brain circadian clock. Trends Neurosci *28*, 145-151.

Aschoff, J. (1965). Response curves in circadian periodicity. In Circadian clocks, J. Aschoff, ed. (North Holland Amsterdam), pp. 95-111.

Aton, S.J., Block, G.D., Tei, H., Yamazaki, S., and Herzog, E.D. (2004). Plasticity of circadian behavior and the suprachiasmatic nucleus following exposure to non-24-hour light cycles. J Biol Rhythms *19*, 198-207.

Aton, S.J., Colwell, C.S., Harmar, A.J., Waschek, J., and Herzog, E.D. (2005). Vasoactive intestinal polypeptide mediates circadian rhythmicity and synchrony in mammalian clock neurons. Nat Neurosci *8*, 476-483.

Balsalobre, A., Damiola, F., and Schibler, U. (1998). A serum shock induces circadian gene expression in mammalian tissue culture cells. Cell *93*, 929-937.

Brancaccio, M., Maywood, E.S., Chesham, J.E., Loudon, A.S., and Hastings, M.H. (2013). A Gq-Ca2+ axis controls circuit-level encoding of circadian time in the suprachiasmatic nucleus. Neuron *78*, 714-728.

Bunger, M.K., Wilsbacher, L.D., Moran, S.M., Clendenin, C., Radcliffe, L.A.,

Hogenesch, J.B., Simon, M.C., Takahashi, J.S., and Bradfield, C.A. (2000). Mop3 is an essential component of the master circadian pacemaker in mammals. Cell *103*, 1009-1017.

Castel, M., Feinstein, N., Cohen, S., and Harari, N. (1990). Vasopressinergic innervation of the mouse suprachiasmatic nucleus: an immuno-electron microscopic analysis. J Comp Neurol *298*, 172-187.

Cheng, M.Y., Bullock, C.M., Li, C., Lee, A.G., Bermak, J.C., Belluzzi, J., Weaver, D.R., Leslie, F.M., and Zhou, Q.Y. (2002). Prokineticin 2 transmits the behavioural circadian rhythm of the suprachiasmatic nucleus. Nature *417*, 405-410.

Chou, T.C., Scammell, T.E., Gooley, J.J., Gaus, S.E., Saper, C.B., and Lu, J. (2003). Critical role of dorsomedial hypothalamic nucleus in a wide range of behavioral circadian rhythms. J Neurosci *23*, 10691-10702.

Doi, M., Ishida, A., Miyake, A., Sato, M., Komatsu, R., Yamazaki, F., Kimura, I., Tsuchiya, S., Kori, H., Seo, K.*, et al.* (2011). Circadian regulation of intracellular G-protein signalling mediates intercellular synchrony and rhythmicity in the suprachiasmatic nucleus. Nat Commun *2*, 327.

Godinho, S.I., Maywood, E.S., Shaw, L., Tucci, V., Barnard, A.R., Busino, L., Pagano, M., Kendall, R., Quwailid, M.M., Romero, M.R.*, et al.* (2007). The *after-hours* mutant reveals a role for Fbxl3 in determining mammalian circadian period. Science *316*, 897-900.

Grima, B., Chelot, E., Xia, R., and Rouyer, F. (2004). Morning and evening peaks of activity rely on different clock neurons of the Drosophila brain. Nature *431*, 869-873.

Hallbeck, M., Hermanson, O., and Blomqvist, A. (1999). Distribution of *preprovasopressin* mRNA in the rat central nervous system. J Comp Neurol *411*,

181-200.

Hamada, T., Antle, M.C., and Silver, R. (2004). Temporal and spatial expression patterns of canonical clock genes and clock-controlled genes in the suprachiasmatic nucleus. Eur J Neurosci *19*, 1741-1748.

Harmar, A.J., Marston, H.M., Shen, S., Spratt, C., West, K.M., Sheward, W.J., Morrison, C.F., Dorin, J.R., Piggins, H.D., Reubi, J.C.*, et al.* (2002). The VPAC(2) receptor is essential for circadian function in the mouse suprachiasmatic nuclei. Cell *109*, 497-508.

Hasegawa, E., Yanagisawa, M., Sakurai, T., and Mieda, M. (2014). Orexin neurons suppress narcolepsy via 2 distinct efferent pathways. J Clin Invest *124*, 604-616.

Hazlerigg, D.G., Ebling, F.J., and Johnston, J.D. (2005). Photoperiod differentially regulates gene expression rhythms in the rostral and caudal SCN. Curr Biol *15*, R449-450.

Helfrich-Forster, C. (2009). Does the morning and evening oscillator model fit better for flies or mice? J Biol Rhythms *24*, 259-270.

Hughes, A.T., Guilding, C., Lennox, L., Samuels, R.E., McMahon, D.G., and Piggins, H.D. (2008). Live imaging of altered period1 expression in the suprachiasmatic nuclei of *Vipr2*$^{-/-}$ mice. J Neurochem *106*, 1646-1657.

Inagaki, N., Honma, S., Ono, D., Tanahashi, Y., and Honma, K. (2007). Separate oscillating cell groups in mouse suprachiasmatic nucleus couple photoperiodically to the onset and end of daily activity. Proc Natl Acad Sci U S A *104*, 7664-7669.

Jagota, A., de la Iglesia, H.O., and Schwartz, W.J. (2000). Morning and evening circadian oscillations in the suprachiasmatic nucleus in vitro. Nat Neurosci *3*, 372-376.

Jin, X., Shearman, L.P., Weaver, D.R., Zylka, M.J., de Vries, G.J., and Reppert, S.M. (1999). A molecular mechanism regulating rhythmic output from the suprachiasmatic

circadian clock. Cell *96*, 57-68.

Kalsbeek, A., Fliers, E., Hofman, M.A., Swaab, D.F., and Buijs, R.M. (2010). Vasopressin and the output of the hypothalamic biological clock. J Neuroendocrinol *22*, 362-372.

Ko, C.H., Yamada, Y.R., Welsh, D.K., Buhr, E.D., Liu, A.C., Zhang, E.E., Ralph, M.R., Kay, S.A., Forger, D.B., and Takahashi, J.S. (2010). Emergence of noise-induced oscillations in the central circadian pacemaker. PLoS Biol *8*, e1000513.

Krashes, M.J., Shah, B.P., Koda, S., and Lowell, B.B. (2013). Rapid versus delayed stimulation of feeding by the endogenously released AgRP neuron mediators GABA, NPY, and AgRP. Cell Metab *18*, 588-595.

Leak, R.K., and Moore, R.Y. (2001). Topographic organization of suprachiasmatic nucleus projection neurons. J Comp Neurol *433*, 312-334.

Li, J.D., Burton, K.J., Zhang, C., Hu, S.B., and Zhou, Q.Y. (2009). Vasopressin receptor V1a regulates circadian rhythms of locomotor activity and expression of clock-controlled genes in the suprachiasmatic nuclei. Am J Physiol Regul Integr Comp Physiol *296*, R824-830.

Li, J.D., Hu, W.P., Boehmer, L., Cheng, M.Y., Lee, A.G., Jilek, A., Siegel, J.M., and Zhou, Q.Y. (2006). Attenuated circadian rhythms in mice lacking the *prokineticin 2* gene. J Neurosci *26*, 11615-11623.

Liu, C., and Reppert, S.M. (2000). GABA synchronizes clock cells within the suprachiasmatic circadian clock. Neuron *25*, 123-128.

Low-Zeddies, S.S., and Takahashi, J.S. (2001). Chimera analysis of the *Clock* mutation in mice shows that complex cellular integration determines circadian behavior. Cell *105*, 25-42.

Lowrey, P.L., and Takahashi, J.S. (2004). Mammalian circadian biology: elucidating genome-wide levels of temporal organization. Annu Rev Genomics Hum Genet *5*, 407-441.

Lu, J., Zhang, Y.H., Chou, T.C., Gaus, S.E., Elmquist, J.K., Shiromani, P., and Saper, C.B. (2001). Contrasting effects of ibotenate lesions of the paraventricular nucleus and subparaventricular zone on sleep-wake cycle and temperature regulation. J Neurosci *21*, 4864-4874.

Madisen, L., Zwingman, T.A., Sunkin, S.M., Oh, S.W., Zariwala, H.A., Gu, H., Ng, L.L., Palmiter, R.D., Hawrylycz, M.J., Jones, A.R.*, et al.* (2010). A robust and high-throughput Cre reporting and characterization system for the whole mouse brain. Nat Neurosci *13*, 133-140.

Masumoto, K.H., Nagano, M., Takashima, N., Hayasaka, N., Hiyama, H., Matsumoto, S., Inouye, S.T., and Shigeyoshi, Y. (2006). Distinct localization of *prokineticin 2* and *prokineticin receptor 2* mRNAs in the rat suprachiasmatic nucleus. Eur J Neurosci *23*, 2959-2970.

Maywood, E.S., Chesham, J.E., O'Brien, J.A., and Hastings, M.H. (2011). A diversity of paracrine signals sustains molecular circadian cycling in suprachiasmatic nucleus circuits. Proc Natl Acad Sci U S A *108*, 14306-14311.

Maywood, E.S., Reddy, A.B., Wong, G.K., O'Neill, J.S., O'Brien, J.A., McMahon, D.G., Harmar, A.J., Okamura, H., and Hastings, M.H. (2006). Synchronization and maintenance of timekeeping in suprachiasmatic circadian clock cells by neuropeptidergic signaling. Curr Biol *16*, 599-605.

Meng, Q.J., Logunova, L., Maywood, E.S., Gallego, M., Lebiecki, J., Brown, T.M., Sladek, M., Semikhodskii, A.S., Glossop, N.R., Piggins, H.D.*, et al.* (2008). Setting

clock speed in mammals: the CK1ε *tau* mutation in mice accelerates circadian pacemakers by selectively destabilizing PERIOD proteins. Neuron *58*, 78-88.

Mickman, C.T., Stubblefield, J.J., Harrington, M.E., and Nelson, D.E. (2008). Photoperiod alters phase difference between activity onset in vivo and mPer2::luc peak in vitro. Am J Physiol Regul Integr Comp Physiol *295*, R1688-1694.

Mieda, M., Williams, S.C., Richardson, J.A., Tanaka, K., and Yanagisawa, M. (2006). The dorsomedial hypothalamic nucleus as a putative food-entrainable circadian pacemaker. Proc Natl Acad Sci USA *103*, 12150-12155.

Molyneux, P.C., Dahlgren, M.K., and Harrington, M.E. (2008). Circadian entrainment aftereffects in suprachiasmatic nuclei and peripheral tissues in vitro. Brain Res *1228*, 127-134.

Muschamp, J.W., Hollander, J.A., Thompson, J.L., Voren, G., Hassinger, L.C., Onvani, S., Kamenecka, T.M., Borgland, S.L., Kenny, P.J., and Carlezon, W.A., Jr. (2014). Hypocretin (orexin) facilitates reward by attenuating the antireward effects of its cotransmitter dynorphin in ventral tegmental area. Proc Natl Acad Sci U S A *111*, E1648-1655.

Pittendrigh, C.S., and Daan, S.A. (1976). Functional analysis of circadian pacemakers in nocturnal rodents: V. Pacemaker structure: a clock for all seasons. J Comp Physiol *106*, 333-355.

Reppert, S.M., and Weaver, D.R. (2002). Coordination of circadian timing in mammals. Nature *418*, 935-941.

Schone, C., Apergis-Schoute, J., Sakurai, T., Adamantidis, A., and Burdakov, D. (2014). Coreleased orexin and glutamate evoke nonredundant spike outputs and computations in histamine neurons. Cell Rep *7*, 697-704.

Shigeyoshi, Y., Taguchi, K., Yamamoto, S., Takekida, S., Yan, L., Tei, H., Moriya, T., Shibata, S., Loros, J.J., Dunlap, J.C., *et al.* (1997). Light-induced resetting of a mammalian circadian clock is associated with rapid induction of the *mPer1* transcript. Cell *91*, 1043-1053.

Shimshek, D.R., Kim, J., Hubner, M.R., Spergel, D.J., Buchholz, F., Casanova, E., Stewart, A.F., Seeburg, P.H., and Sprengel, R. (2002). Codon-improved Cre recombinase (iCre) expression in the mouse. Genesis *32*, 19-26.

Siepka, S.M., Yoo, S.H., Park, J., Song, W., Kumar, V., Hu, Y., Lee, C., and Takahashi, J.S. (2007). Circadian mutant *Overtime* reveals F-box protein FBXL3 regulation of *cryptochrome* and *period* gene expression. Cell *129*, 1011-1023.

Silver, R., Romero, M.T., Besmer, H.R., Leak, R., Nunez, J.M., and LeSauter, J. (1996). Calbindin-D28K cells in the hamster SCN express light-induced Fos. Neuroreport *7*, 1224-1228.

Stoleru, D., Peng, Y., Agosto, J., and Rosbash, M. (2004). Coupled oscillators control morning and evening locomotor behaviour of Drosophila. Nature *431*, 862-868.

Storch, K., Paz, C., Signorovitch, J., Raviola, E., Pawlyk, B., Li, T., and Weitz, C. (2007). Intrinsic Circadian Clock of the Mammalian Retina: Importance for Retinal Processing of Visual Information. Cell *130*, 730-741.

Visel, A., Carson, J., Oldekamp, J., Warnecke, M., Jakubcakova, V., Zhou, X., Shaw, C.A., Alvarez-Bolado, G., and Eichele, G. (2007). Regulatory pathway analysis by high-throughput in situ hybridization. PLoS Genet *3*, 1867-1883.

Webb, A.B., Angelo, N., Huettner, J.E., and Herzog, E.D. (2009). Intrinsic, nondeterministic circadian rhythm generation in identified mammalian neurons. Proc Natl Acad Sci U S A *106*, 16493-16498.

Welsh, D.K., Takahashi, J.S., and Kay, S.A. (2010). Suprachiasmatic nucleus: cell autonomy and network properties. Annu Rev Physiol *72*, 551-577.

Yamaguchi, Y., Suzuki, T., Mizoro, Y., Kori, H., Okada, K., Chen, Y., Fustin, J.M., Yamazaki, F., Mizuguchi, N., Zhang, J.*, et al.* (2013). Mice genetically deficient in vasopressin V1a and V1b receptors are resistant to jet lag. Science *342*, 85-90.

Yoo, S.H., Yamazaki, S., Lowrey, P.L., Shimomura, K., Ko, C.H., Buhr, E.D., Siepka, S.M., Hong, H.K., Oh, W.J., Yoo, O.J.*, et al.* (2004). PERIOD2::LUCIFERASE real-time reporting of circadian dynamics reveals persistent circadian oscillations in mouse peripheral tissues. Proc Natl Acad Sci U S A *101*, 5339-5346.

FIGURE LEGENDS

Figure 1. Generation of mice lacking *Bmal1* specifically in AVP neuron (*Avp-Bmal1*$^{-/-}$ mice). (A) Cre-mediated recombination was specific to AVP neurons in the SCN of *Avp-Cre* mice crossed with *Rosa26-tdTomato* Cre-dependent reporter mice. Coronal brain sections were immunostained for AVP (upper layers) or VIP (lower layers) in green. (B) BMAL1 expression in the SCN of *Avp-Cre* mice was drastically reduced specifically in AVP neurons. Coronal brain sections prepared from control and *Avp-Bmal1*$^{-/-}$ mice crossed with *Rosa26-tdTomato* reporter mice were immunostained for BMAL1. AVP neurons were identified as tdTomato+ cells. The locations of the magnified images are indicated by white rectangles in the low-power images. Scale bars, 100 μm. 3v, third ventricle. See also Figure S1.

Figure 2. *Avp-Bmal1*$^{-/-}$ mice show lengthenings of the free-running period and the activity time. (A) Representative locomotor activity of one control and two *Avp-Bmal1*$^{-/-}$ mice. Animals were initially housed in 12:12-h light/dark (LD) conditions and then transferred to constant darkness (DD). Gray shading indicates the time when lights were off. (B) Daily profile of locomotor activity in LD or DD, including the mean free-running period and the activity time in DD. Values for activity in DD were calculated for data on days 15–29 in DD. Free-running period and activity time were increased in *Avp-Bmal1*$^{-/-}$ mice. In this and subsequent figures, error bars indicate S.E.M. n = 9 for control, n = 8 for *Avp-Bmal1*$^{-/-}$ mice. ***, $p < 0.001$. (C) Hourly plot of time spent in wakefulness in LD or DD (days 8–10). n = 4 for control, n = 5 for *Avp-Bmal1*$^{-/-}$ mice. *, $p < 0.05$. See also Figure S2 and Table S1.

Figure 3. *Avp-Bmal1*$^{-/-}$ mice show diminished photoperiodic response to the long-day condition and transient arrhythmicity in the subsequent DD. (A) Representative locomotor activity. Animals were initially housed in LD12:12, then in LD18:6, and finally transferred to constant darkness (DD). (B) Daily profile of locomotor activity in LD12:12 or LD18:6 (for the last 7 days in each condition). n = 8. (C) Mean periodogram for days 1–7 or 12–19 in DD immediately following LD18:6. *Avp-Bmal1*$^{-/-}$ mice showed drastically attenuated rhythmicity on days 1–7 in DD.

Figure 4. *Avp-Bmal1*$^{-/-}$ mice reentrain faster after the shifts of the LD cycle than controls. (A) Representative locomotor activity of control and *Avp-Bmal1*$^{-/-}$ mice upon a 4-hr phase shift of the LD cycle. (B) Number of days required for reentrainment to the 4-hr phase shift. n = 8. (C) Representative locomotor activity upon an 8-hr phase shift of the LD cycle. A small number of control mice (2 of 7) reentrained to the 8-hr phase advance by delaying their activity rhythm (lower panel). (D) Number of days required for reentrainment to the 8-hr phase shift, which was reduced in *Avp-Bmal1*$^{-/-}$ mice. n = 7 for phase advance; n = 3 or 4 for control or *Avp-Bmal1*$^{-/-}$ mice for phase delay. *, $p < 0.05$; **, $p < 0.01$. (E) Mean periodogram for the first 5 days immediately after the 8-hr phase advance (indicated by a vertical bar in C), showing attenuated circadian rhythmicity in *Avp-Bmal1*$^{-/-}$ mice.

Figure 5. Light-responsiveness of the SCN is attenuated in *Avp-Bmal1*$^{-/-}$ mice. (A) Representative locomotor activity of control and *Avp-Bmal1*$^{-/-}$ mice with or without a 30-min light pulse at ZT14. Mice were initially housed in LD12:12 and then transferred to DD after the light pulse. (B) Phase delay induced by a 30-min light pulse at ZT14

(indicated by orange asterisks); the delay was decreased in *Avp-Bmal1*$^{-/-}$ mice. n = 8. ***, $p < 0.001$. (C) Representative images of *Per1* mRNA expression at ZT15 in the SCN of control and *Avp-Bmal1*$^{-/-}$ mice with or without a 30-min light pulse at ZT14. Coronal brain sections were hybridized in situ to a *Per1* antisense probe. Scale bar, 100 μm. (D) *Per1* expression in the dorsal or ventral SCN induced by a 30-min light pulse at ZT14; this induction in the ventral SCN was decreased in *Avp-Bmal1*$^{-/-}$ mice. Representative regions defined as the dorsal and ventral SCN are indicated by yellow circles in (C). n = 4. ggg, effect of genotype; lll, effect of light; $p < 0.001$. Interaction between genotype and light was also statistically significant ($p < 0.001$) in the ventral SCN.

Figure 6. Circadian gene expression is attenuated in the dorsal SCN of *Avp-Bmal1*$^{-/-}$ mice. (A) Representative images of *Per1*, *Avp*, *Prok2*, *Rgs16*, and *Vip* mRNA expression in the SCN of control and *Avp-Bmal1*$^{-/-}$ mice at the time indicated. Coronal brain sections were hybridized in situ to an antisense probe for each gene. Scale bar, 100 μm. (B) Circadian expression of each gene in the dorsal or ventral SCN. Representative regions defined as the dorsal and ventral SCN are indicated by yellow circles in (A). n = 3. ggg, interaction between genotype and expression; rrr, interaction between the region within the SCN and expression, $p < 0.001$. See also Figure S3.

Figure 7. The period of cellular circadian oscillation is variable and lengthened in the dorsal SCN of *Avp-Bmal1*$^{-/-}$ mice. (A) Representative circadian rhythm of PER2::LUC at the SCN tissue level of one control and two *Avp-Bmal1*$^{-/-}$ mice housed in DD. The right example represents a minority of *Avp-Bmal1*$^{-/-}$ mice that demonstrated oscillation

with relatively large amplitude. (B) Periods of the first and second cycle, and the average of the first three cycles (3d ave). Definition of the cycles is indicated in (A). *, $p < 0.05$; **, $p < 0.01$; ***, $p < 0.001$. n = 14 for control, n = 15 for *Avp-Bmal1*$^{-/-}$ mice. (C) Representative amplitude and period maps of PER2::LUC oscillation at the pixel level of the SCN slices of the mid-rostrocaudal region prepared from mice housed in DD. Amplitudes and periods of PER2::LUC oscillations in the individual pixels covering the SCN were calculated by cosine curve fittings on the data for 25–72 hr after slice preparations. Scale bar, 100 μm. (D) Relative frequency of individual pixels' amplitudes was calculated for each slice (mouse), and the mean relative frequency for each genotype is shown. (E) Relative frequency of individual pixels' periods. Distribution of period was broader with considerable number of pixels with longer periods in the dorsal SCN of *Avp-Bmal1*$^{-/-}$ mice. Mean (F) and SD (G) of the periods of individual pixels' oscillations in the dorsal or ventral SCN. In addition to the values calculated from the data for 25–72 hr after slice preparations, the same parameters for 49–96 hr are shown for comparison. In the dorsal SCN of *Avp-Bmal1*$^{-/-}$ mice, the SD of period increased stably, whereas the mean of period increased transiently (25–72 hr). (D)-(G): n = 6 for control, n = 7 for *Avp-Bmal1*$^{-/-}$ mice. For (D) and (E), ggg, interaction between genotype and amplitude/period; rrr, interaction between the region within the SCN and amplitude/period, $p < 0.001$. For (F), g, effect of genotype; r, effect of the region within the SCN; t, effect of time window; one letter, $p < 0.05$; two letters, $p < 0.01$; three letters, $p < 0.001$. See also Figure S4.

Figure 1

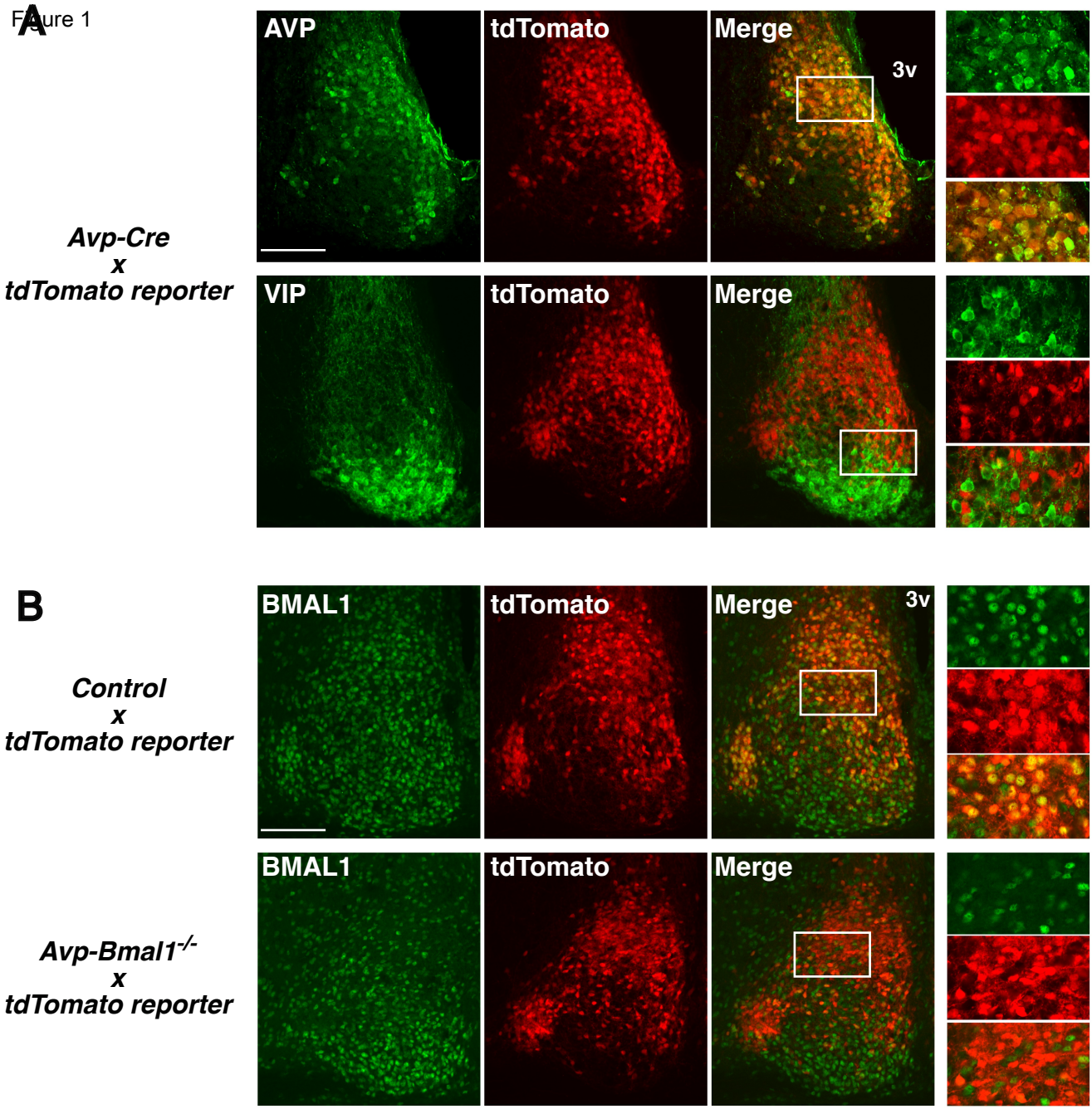
A
AVP
tdTomato
Merge
3v
Avp-Cre
x
tdTomato reporter
VIP
tdTomato
Merge
B
BMAL1
tdTomato
Merge
3v
Control
x
tdTomato reporter
BMAL1
tdTomato
Merge
Avp-Bmal1-/-
x
tdTomato reporter

Figure 2

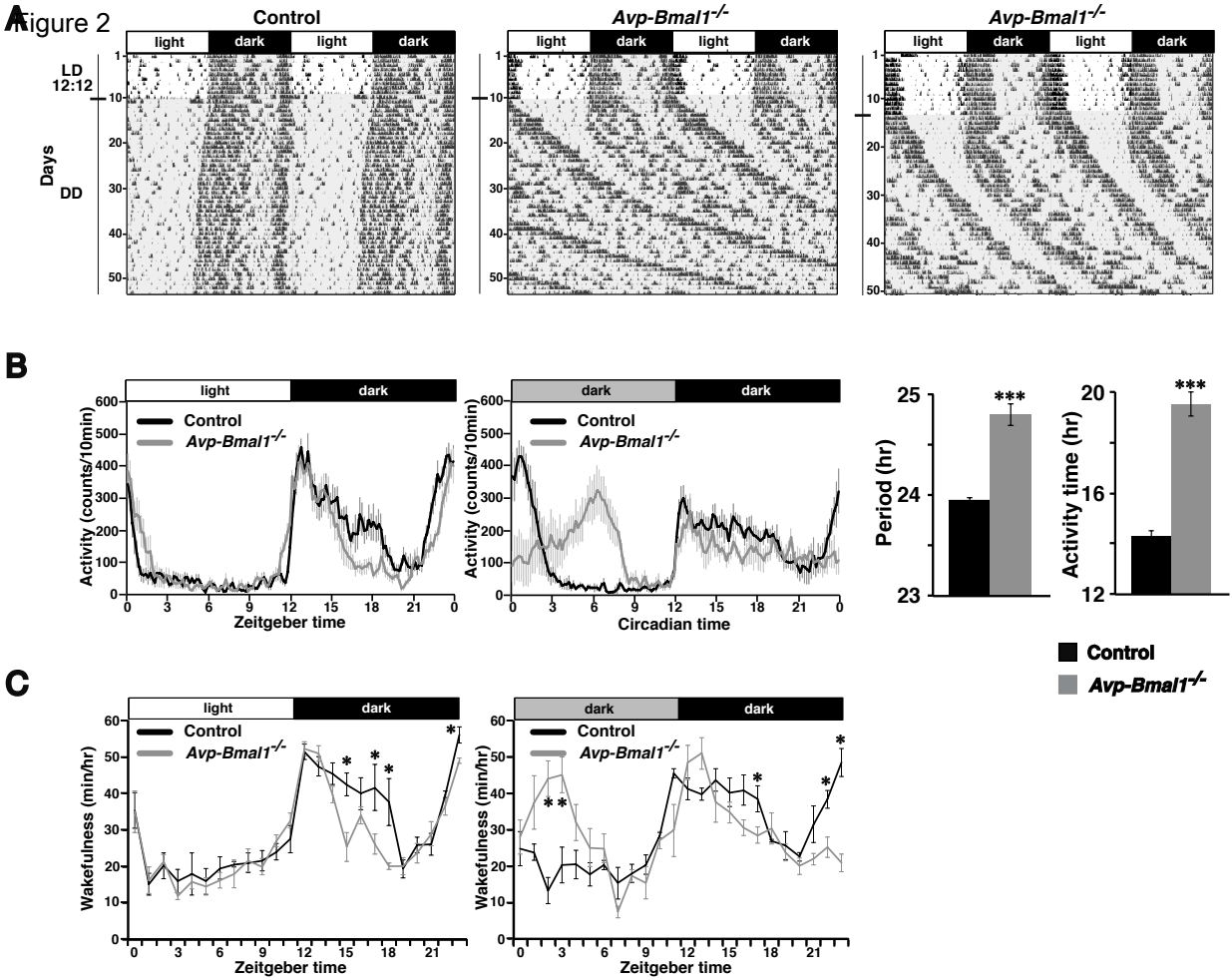
A
Control
Avp-Bmal1-/-
Avp-Bmal1-/-
light
dark
light
dark
LD
12:12
Days
DD
B
light
dark
dark
dark
Control
Avp-Bmal1-/-
Activity (counts/10min)
Zeitgeber time
Circadian time
Period (hr)
Activity time (hr)
***
***
Control
Avp-Bmal1-/-
C
Wakefulness (min/hr)
Zeitgeber time
**

Figure 3

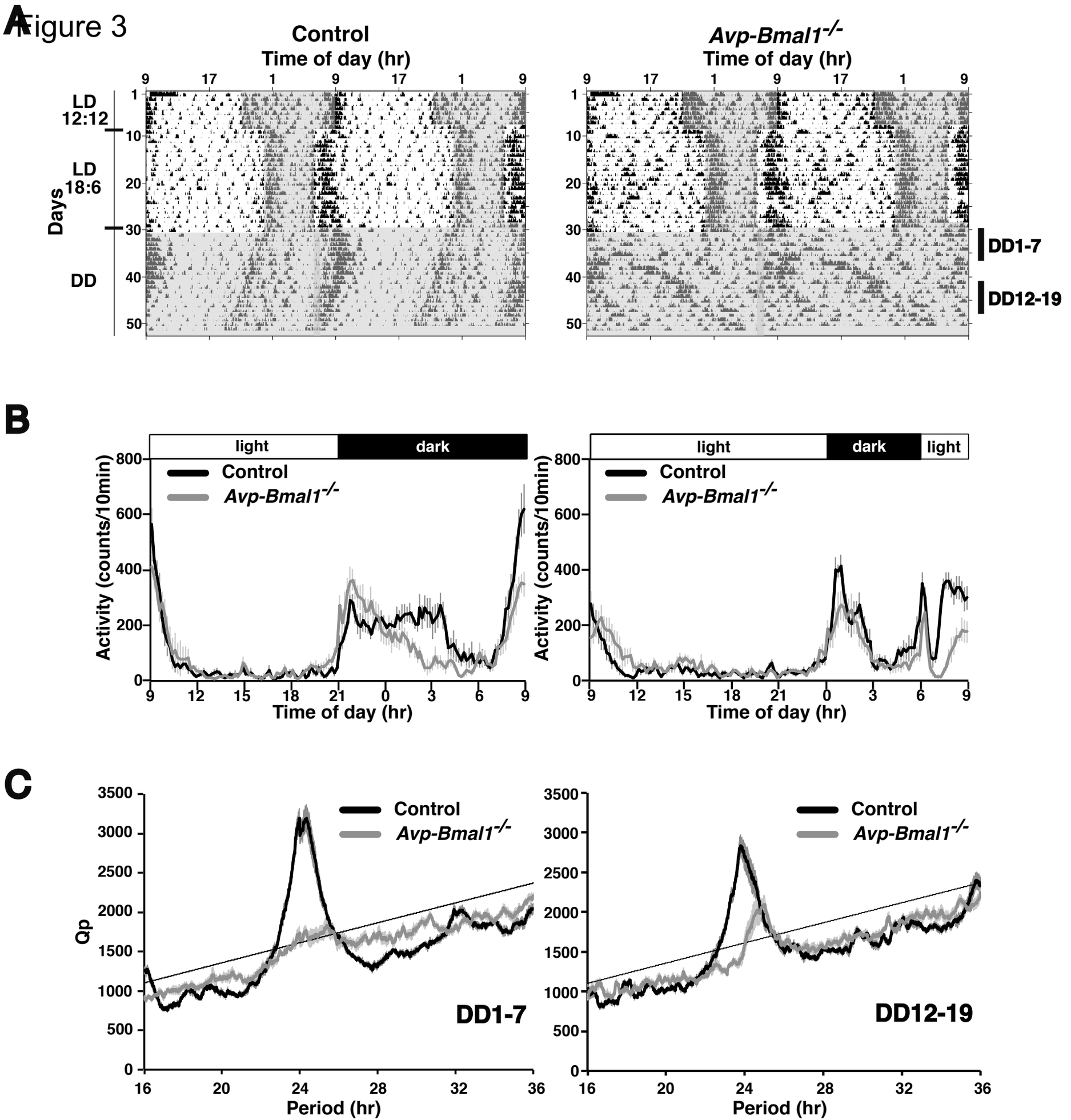
A
Control
Time of day (hr)
Avp-Bmal1-/-
LD 12:12
LD 18:6
DD
Days
DD1-7
DD12-19
B
light
dark
Control
Avp-Bmal1-/-
Activity (counts/10min)
Time of day (hr)
C
Qp
Period (hr)
DD1-7
DD12-19

Figure 4

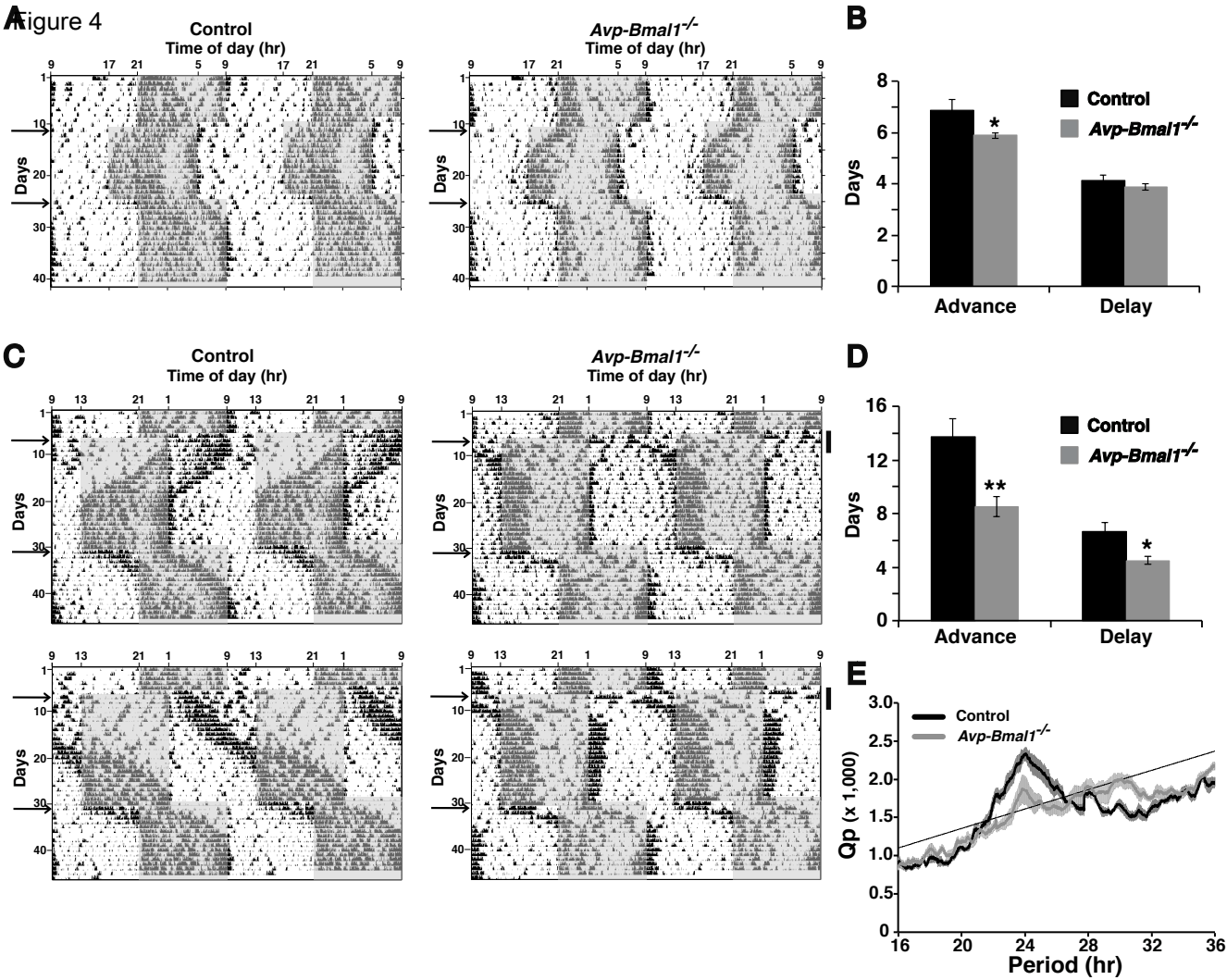
A
Control
Time of day (hr)
9 17 21 5 9 17 21 5 9
Days
1 10 20 30 40
Avp-Bmal1-/-
Time of day (hr)
9 17 21 5 9 17 21 5 9
Days
1 10 20 30 40
B
Days
0 2 4 6 8
Control
Avp-Bmal1-/-
*
Advance
Delay
C
Control
Time of day (hr)
9 13 21 1 9 13 21 1 9
Days
1 10 20 30 40
Avp-Bmal1-/-
Time of day (hr)
9 13 21 1 9 13 21 1 9
Days
1 10 20 30 40
D
Days
0 4 8 12 16
Control
Avp-Bmal1-/-
**
*
Advance
Delay
E
Qp (x 1,000)
0 0.5 1.0 1.5 2.0 2.5 3.0
Control
Avp-Bmal1-/-
16 20 24 28 32 36
Period (hr)

Figure 5

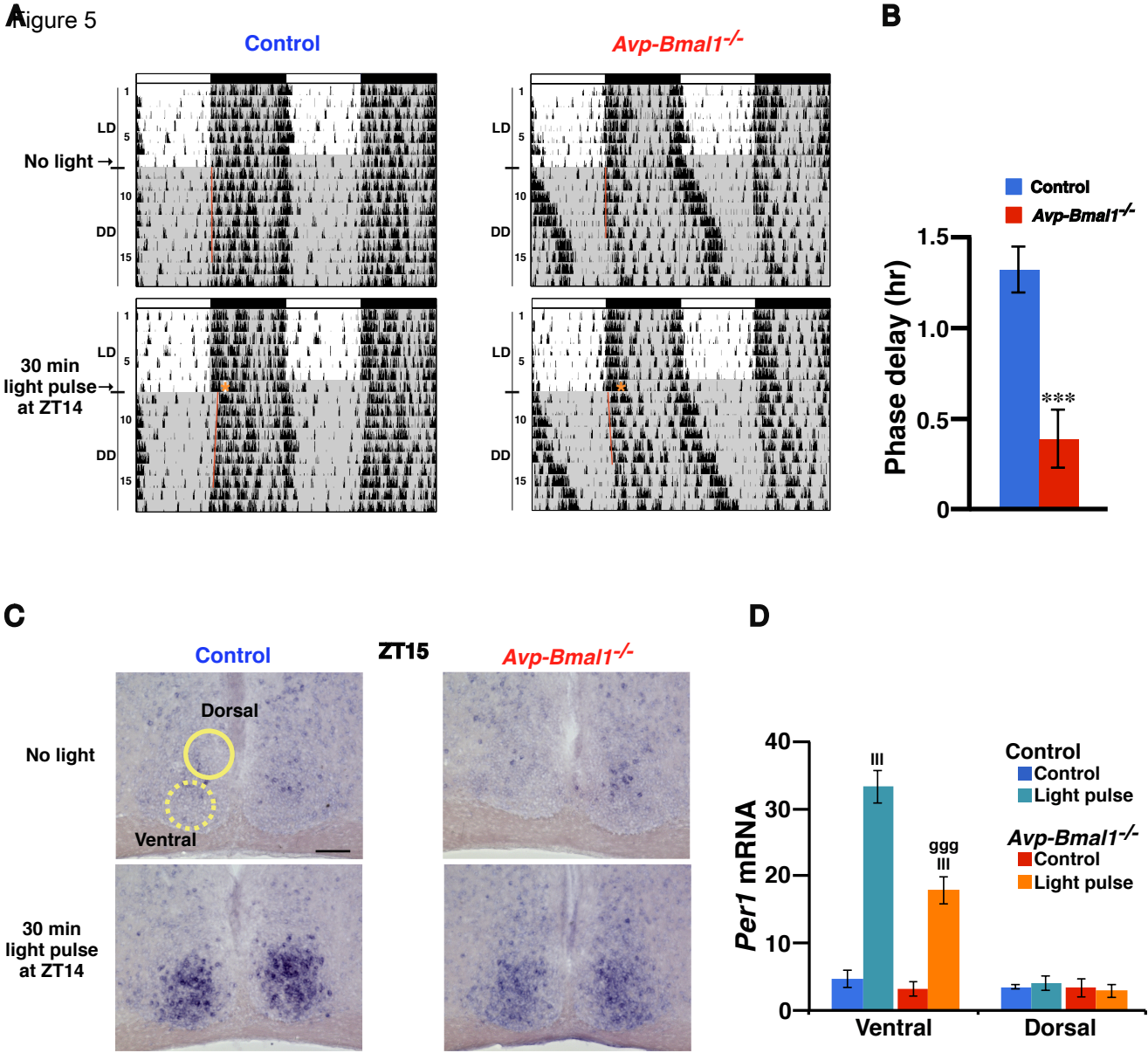
A
Control
Avp-Bmal1-/-
No light
30 min light pulse at ZT14
LD
DD
B
Control
Avp-Bmal1-/-
Phase delay (hr)
1.5
1.0
0.5
0
***
C
Control
ZT15
Avp-Bmal1-/-
No light
30 min light pulse at ZT14
Dorsal
Ventral
D
Per1 mRNA
40
30
20
10
0
III
ggg III
Control
Control
Light pulse
Avp-Bmal1-/-
Control
Light pulse
Ventral
Dorsal

Figure 6

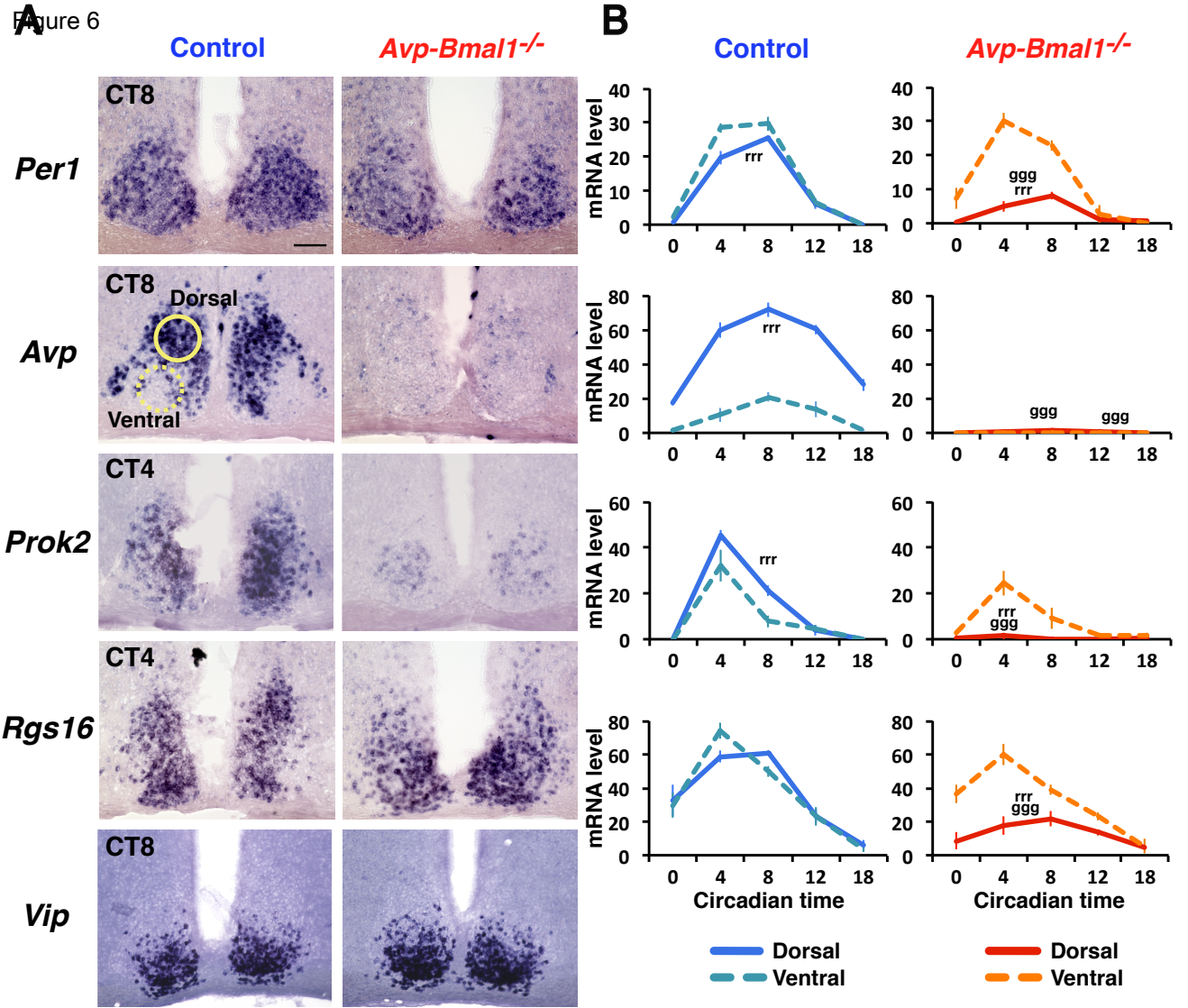
A
Control
Avp-Bmal1-/-
Per1
Avp
Prok2
Rgs16
Vip
CT8
CT4
Dorsal
Ventral
B
Control
Avp-Bmal1-/-
mRNA level
Circadian time
rrr
ggg
Dorsal
Ventral

Figure 7

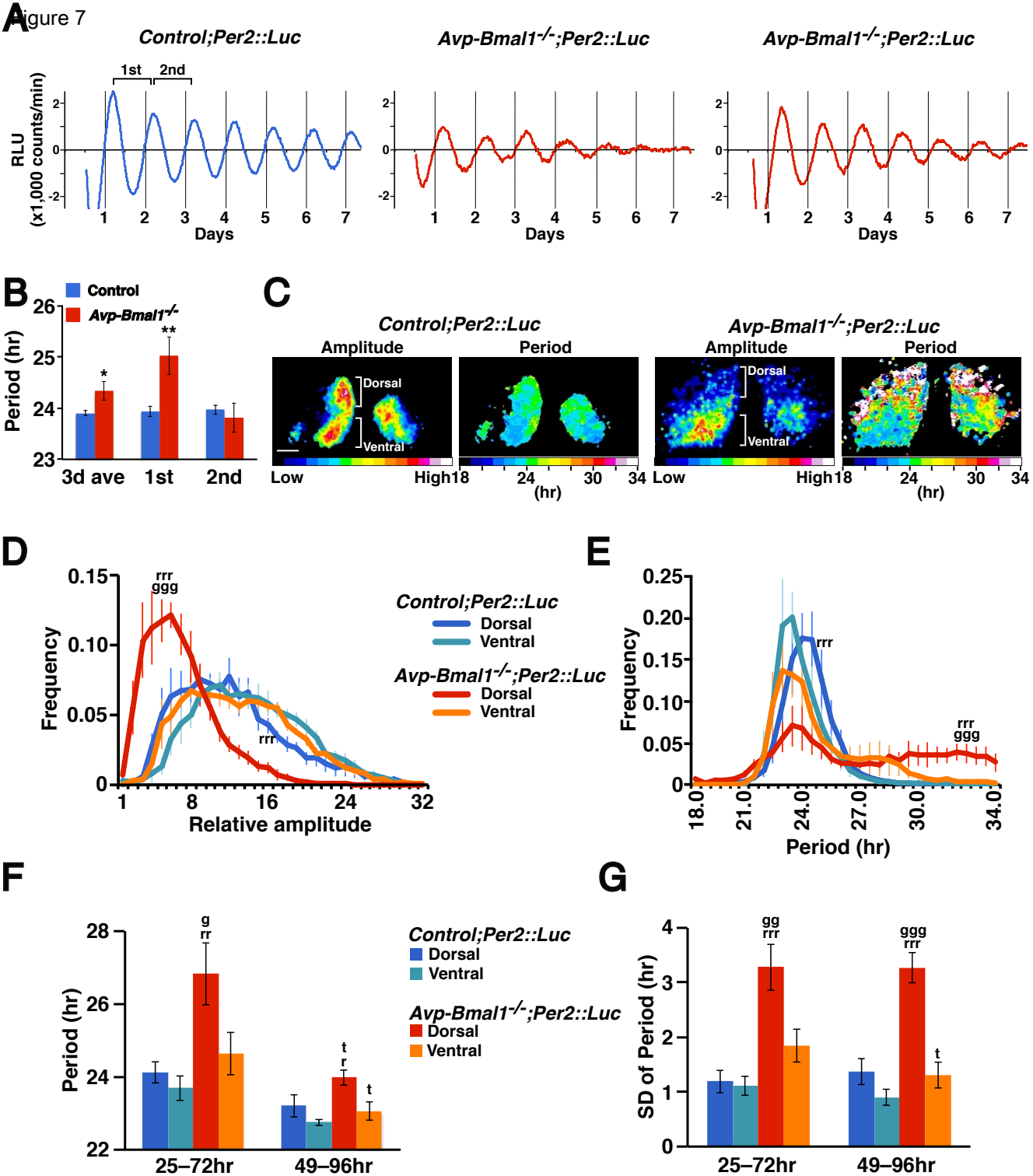
A
Control;Per2::Luc
Avp-Bmal1-/-;Per2::Luc
Avp-Bmal1-/-;Per2::Luc
1st
2nd
RLU
(x1,000 counts/min)
Days
B
Control
Avp-Bmal1-/-
Period (hr)
3d ave
1st
2nd
C
Control;Per2::Luc
Avp-Bmal1-/-;Per2::Luc
Amplitude
Period
Dorsal
Ventral
Low
High
(hr)
D
Frequency
Relative amplitude
rrr
ggg
Control;Per2::Luc
Dorsal
Ventral
Avp-Bmal1-/-;Per2::Luc
Dorsal
Ventral
E
Frequency
Period (hr)
F
Period (hr)
25–72hr
49–96hr
G
SD of Period (hr)
25–72hr
49–96hr

INVENTORY OF SUPPREMENTAL INFORMATION

SUPPLEMENTAL FIGURES

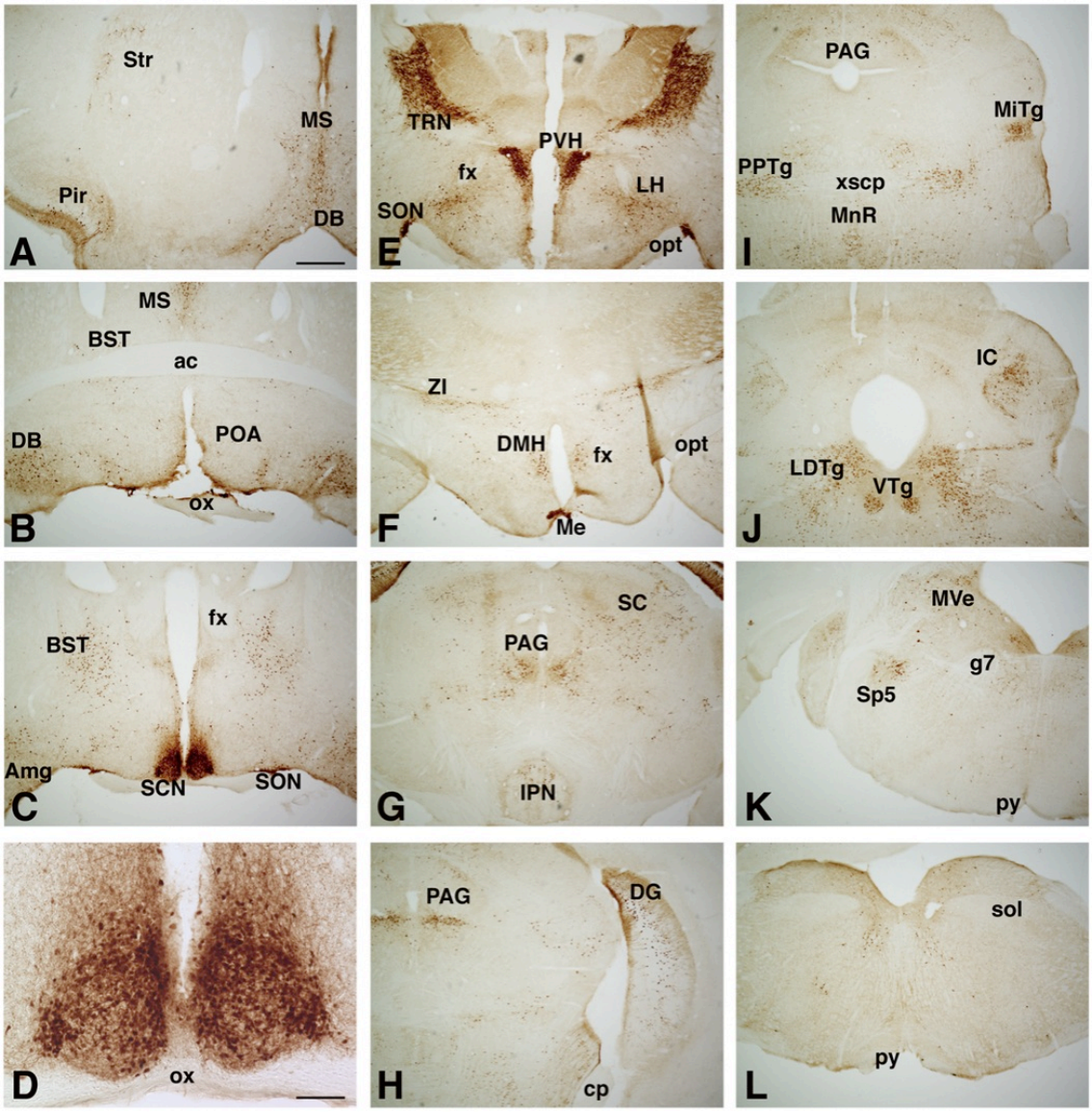

Figure S1. Distribution of cells with Cre-mediated recombination in *Avp-Cre* mice crossed with *Rosa26-tdTomato* reporter mice, related to Figure 1. Coronal sections from rostral (A) to caudal (L) were immunostained for tdTomato. (D) is a magnified image of the SCN in (C). Note that tdTomato expression level did not necessarily correlate with Cre expression level, because tdTomato expression was driven by strong *Rosa26-CAG* promoter activity once the floxed transcriptional blocker was deleted, which could occur with a low level of Cre expression. Thus, Cre expression in tdTomato+ cells might not necessarily be sufficient to delete both $Bmal1^{fl}$ alleles in $Avp\text{-}Bmal1^{-/-}$ mice. Scale bars, 100 μm for D; 500 μm for other panels. ac, anterior commissure; Amyg,

anterior amygdala; BST, bed nucleus of the stria terminalis; DB, diagonal band; cp, cerebral peduncle; DG, dentate gyrus; DMH, dorsomedial hypothalamic nucleus; fx, fornix; g7, genu of the facial nerve; IC, inferior colliculus; IPN, interpeduncular nucleus; LDTg, laterodorsal tegmental nucleus; LH, lateral hypothalamus; Me, medial eminence; MiTg, microcellular tegmental nucleus; MnR, median raphe nucleus; MS, medial septal nucleus; MVe, medial vestibular nucleus; opt, optic tract; ox, optic chiasm; PAG, periaqueductal gray; Pir, piriform cortex; PPTg, pedunculopontine tegmental nucleus; POA, preoptic area; PVH, paraventricular hypothalamic nucleus; py, pyramidal tract; SC, superior colliculus; SCN, suprachiasmatic nucleus; sol, solitary tract; SON, supraoptic nucleus; Sp5, spinal trigeminal nucleus; Str, striatum; TRN, thalamic reticular nucleus; VTg, ventral tegmental nucleus; xscp, decussation of the superior cerebellar peduncle; ZI, zona incerta (Paraxinos and Franklin, The Mouse Brain, 2001).

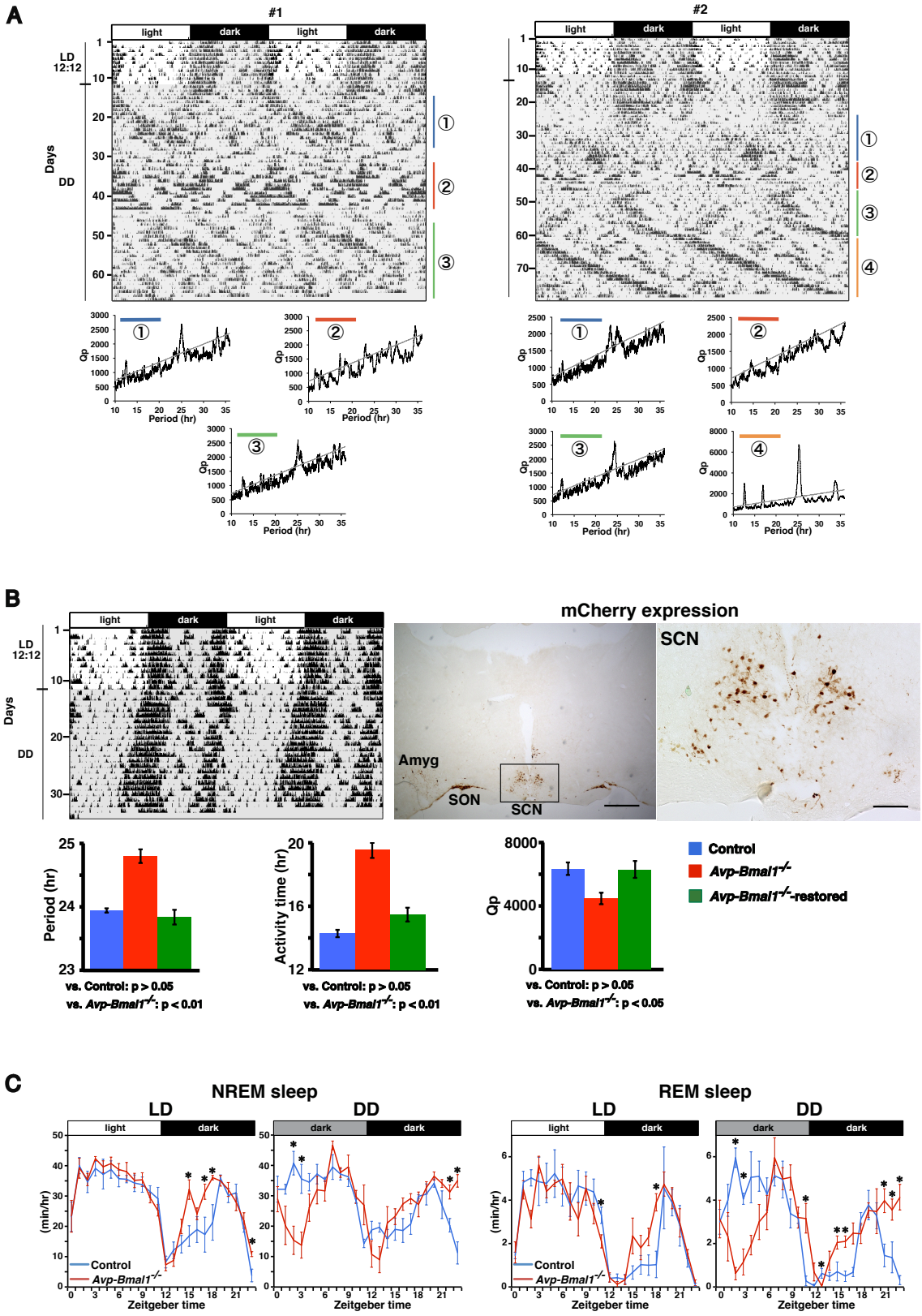

Figure S2. Circadian phenotype of *Avp-Bmal1*$^{-/-}$ mice, related to Figure 2. (A) Examples of *Avp-Bmal1*$^{-/-}$*;Per2::Luc* mice showing the unique and severely impaired

pattern of locomotor activity observed in 3 out of 21 *Avp-Bmal1*$^{-/-}$*;Per2::Luc* mice. Free-running rhythms were highly unstable. In mouse #1, onset and offset components of activity free-ran with shorter and longer periods, respectively, when released into DD, after which they merged. This mouse then showed transient arrhythmicity, followed by the reappearance of rhythmicity with a lengthened period. Mouse #2 also showed transient arrhythmicity and multiple free-running activity components with different periods, and it then recovered a rhythmicity with lengthened period. Periodograms corresponding to the durations indicated by colored vertical bars and circled numbers beside actograms are also shown. (B) Restoration of *Bmal1* expression in the SCN AVP neurons of adult *Avp-Bmal1*$^{-/-}$ mice reversed their circadian phenotype. Mixture of recombinant AAV vectors expressing *Bmal1* or *mCherry* in a Cre-dependent manner by means of DIO (doublefloxed inverse open reading frame) was focally injected into the SCN. The ratio of AAV-Bmal1ext-DIO-Bmal1 to AAV-EF1α-DIO-mCherry was 5:1. Locomotor activity and mCherry expression of a representative mouse with *Bmal1* restoration, mean free-running period, activity time, and amplitude (Qp values by periodogram analysis) are shown. Values are mean ± S.E.M. (n = 9 for control, n = 8 for *Avp-Bmal1*$^{-/-}$, n = 5 for *Avp-Bmal1*$^{-/-}$ mice with *Bmal1* restoration; for the former two, data from Figure 2 are included for comparison). The number of mCherry+ cells in the SCN of restored mice was 115 ± 8 cells/slice. Off-target restoration of *Bmal1* was observed in the SON of all mice examined, and in scattered cells of a few brain regions, including the PVH, anterior amygdala, and the reticular thalamus, in some mice, not all. Scale bars, 500 μm for middle panel; 100 μm for right panel. (C) Hourly plots of time spent in NREM or REM sleep in LD or DD (days 8–10). (n = 4 for control, n = 5 for *Avp-Bmal1*$^{-/-}$ mice). *, $p < 0.05$.

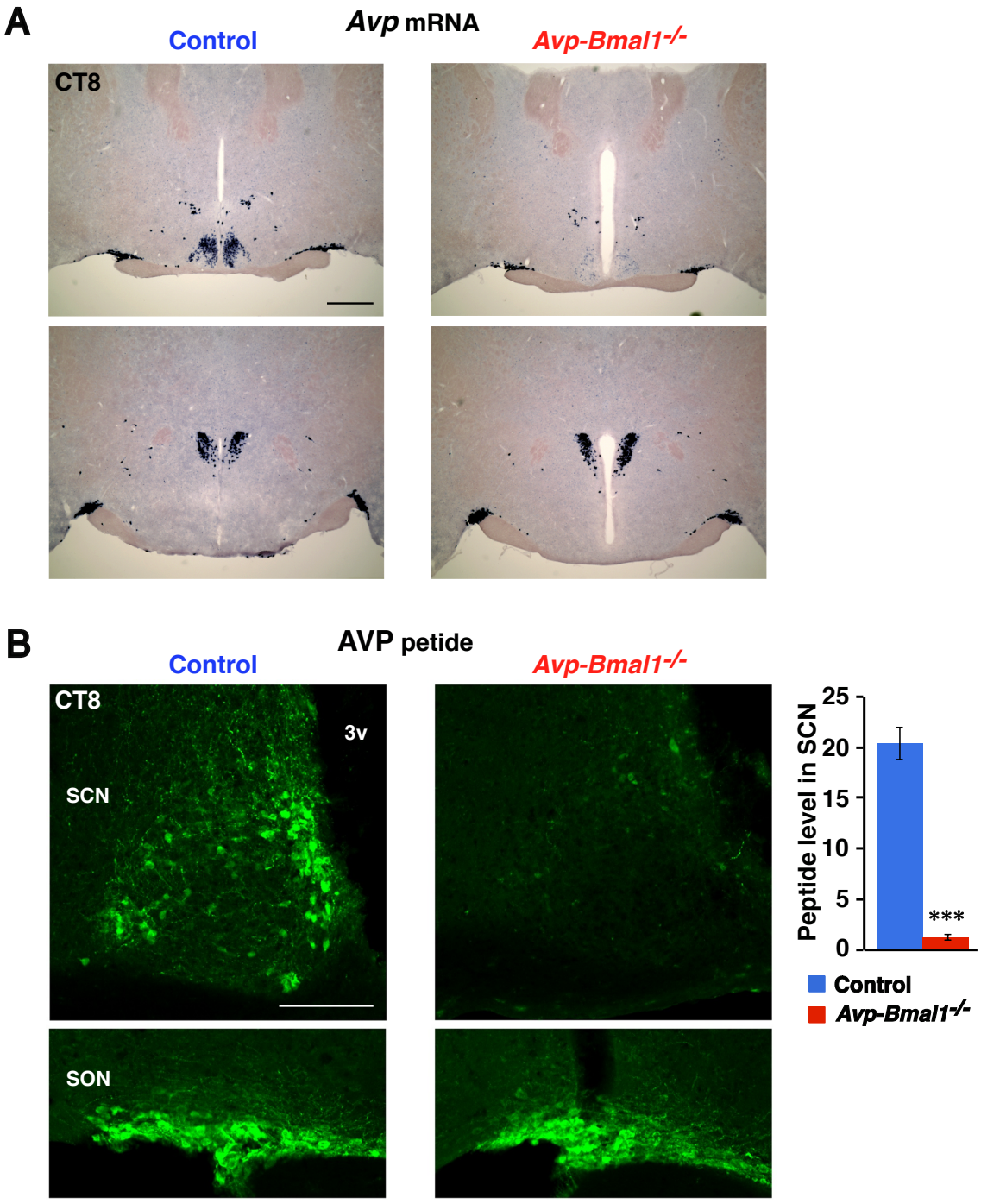

Figure S3. Expression of *Avp* mRNA and AVP peptide in the PVH and SON is normal, whereas that in the SCN is drastically reduced in *Avp-Bmal1*$^{-/-}$ mice, related to Figure 6. (A) *Avp* mRNA expression. Coronal brain sections from control and *Avp-Bmal1*$^{-/-}$ mice were in situ hybridized to an antisense probe for *Avp*. (B) AVP peptide expression. Coronal brain sections were immunostained for AVP. Thus, BMAL1-dependent transcription of *Avp* gene is specific to the SCN. Nevertheless, we still observed a small

number of cells expressing *Avp* mRNA or AVP peptide at low levels in the SCN of *Avp-Bmal1*$^{-/-}$ mice, which is consistent with the fact that these mice still retain a small number of SCN AVP neurons with BMAL1 expression. Scale bar, 500 μm for A; 100 μm for B. ***, $p < 0.001$.

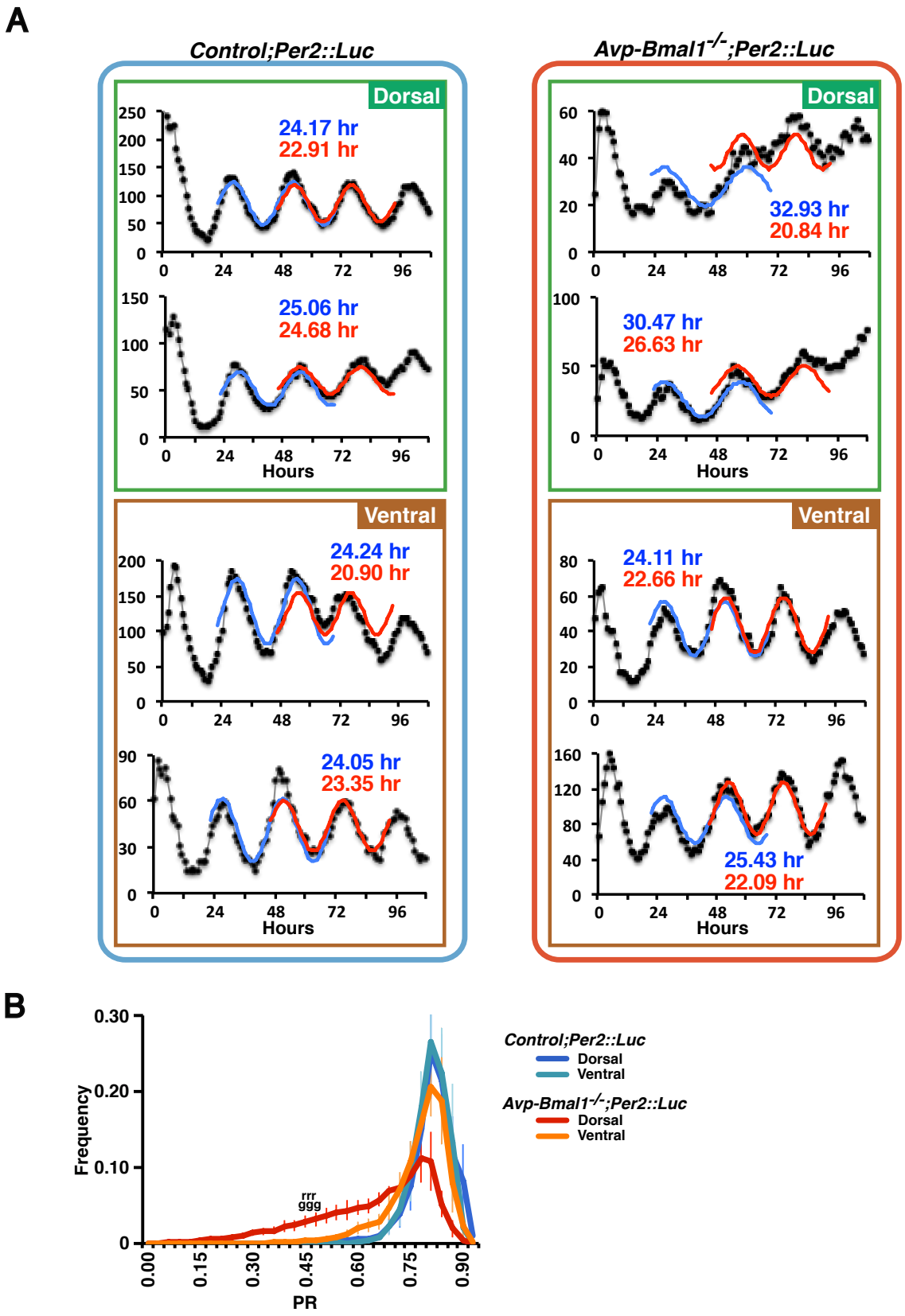

Figure S4. Period of cellular circadian oscillation is highly variable in the dorsal SCN

of *Avp-Bmal1*$^{-/-}$ mice, related to Figure 7. (A) Examples of cosine curve fittings for PER2::LUC oscillations of individual pixels (2 examples each for the dorsal and ventral SCN of *Control;Per2::Luc* and *Avp-Bmal1*$^{-/-}$*;Per2::Luc* mice). For each example, the raw data are shown as black squares. Cosine curve fittings were performed on the data for 25–72 hours (blue curve superimposed on the raw data) and 49–96 hours (red curve) after slice preparations to evaluate temporal stability of period (note that values labeling the X-axis of each graph represent hours after the initiation of recording). Calculated periods for these two time windows are also indicated in the corresponding colors. (B) Relative frequency of individual pixels' percent rhythms (PR; percentage of overall variance attributed to the best fitted cosine curve) was calculated for each slice (mouse), and the mean relative frequency for each genotype is shown. Values are mean ± S.E.M. (n = 6 for control, n = 7 for *Avp-Bmal1*$^{-/-}$ mice). ggg, interaction between genotype and amplitude/period; rrr, interaction between the region within the SCN and PR, $p < 0.001$.

Table S1. Phenotypic Characteristics of *Avp-Bmal1*$^{-/-}$ Mice

Genotype	*Avp-Bmal1*$^{-/-}$	Control	*Bmal1*$^{fl/fl}$	*Avp-Cre;Bmal1*$^{wt/fl}$
n	8	9 (*Bmal1*$^{fl/fl}$&*Avp-Cre;Bmal1*$^{wt/fl}$)	5	4
Light-Dark (7 days)				
Amplitude (Qp)	3903.95 ± 277.46	3814.61 ± 104.45	3824.66 ± 86.42	3802.05 ± 230.05
Activity time (hr)	14.16 ± 0.31	12.94 ± 0.22**	12.65 ± 0.18*	13.31 ± 0.41
Activity onset (ZT)	11.24 ± 0.12	11.87 ± 0.05***	11.89 ± 0.04**	11.85 ± 0.11**
Activity offset (ZT)	1.40 ± 0.26	0.81 ± 0.22	0.54 ± 0.17	1.15 ± 0.42
Activity (count)				
Dark period	13404 ± 1292	17536 ± 1352*	18776 ± 1811	15987 ± 2016
Light period	5375 ± 559	3874 ± 520	3444 ± 202	4411 ± 1176
24 hr	18778 ± 1457	21410 ± 1479	22220 ± 1789	20397 ± 2680
Constant Darkness (days 15-29)				
Amplitude (Qp)	4484.99 ± 370.51	6334.72 ± 396.61**	6240.82 ± 500.17	6452.10 ± 720.14*
Free-running period (hr)				
Periodogram	24.80 ± 0.11	23.94 ± 0.03***	24.00 ± 0.03**	23.87 ± 0.04**
FFT	25.70 ± 0.56	24.00 ± 0.00**	24.00 ± 0.00	24.00 ± 0.00
Visual inspection				
Activity onset	24.79 ± 0.08	23.92 ± 0.04***	24.00 ± 0.02**	23.83 ± 0.04**
Activity offset	24.81 ± 0.10	23.96 ± 0.03***	24.01 ± 0.03**	23.90 ± 0.02**
Activity time (hr)				
Activity profile	19.52 ± 0.47	14.29 ± 0.24***	14.08 ± 0.36**	14.56 ± 0.30**
Visual inspection	19.35 ± 0.45	14.10 ± 0.21***	13.90 ± 0.29**	14.35 ± 0.30**
Cycle-to-cycle variability (SD) (min) – Visual inspection				
Activity onset	43.65 ± 4.50	15.33 ± 1.23***	14.04 ± 1.45**	16.95 ± 1.98**
Activity offset	59.70 ± 9.50	23.80 ± 2.10**	25.56 ± 3.41*	21.60 ± 2.05*
Activity (count)				
Activity period	18610 ± 1357	18601 ± 1346	19043 ± 1324	18048 ± 2787
Rest period	1232 ± 302	1839 ± 247	1733 ± 231	1972 ± 516
Free-running period	19842 ± 1518	20440 ± 1476	20776 ± 1407	20020 ± 3108
Constant Darkness (days 1-7)				
Free-running period (hr) – Visual inspection				
Activity onset	24.01 ± 0.02	23.90 ± 0.04*	23.93 ± 0.05	23.87 ± 0.05
Activity offset	24.59 ± 0.08	24.02 ± 0.03***	24.07 ± 0.03**	24.00 ± 0.04**

Values are mean ± S.E.M. Effects of genotype were analyzed by Student's t-tests for comparison between *Avp-Bmal1*$^{-/-}$ and control mice, or by one-way repeated-measures ANOVA and Tukey-HSD *post hoc* tests for comparison between *Avp-Bmal1*$^{-/-}$, *Bmal1*$^{fl/fl}$, and *Avp-Cre;Bmal1*$^{wt/fl}$ mice. *, $p < 0.05$; **, $p < 0.01$; ***, $p < 0.001$; vs. *Avp-Bmal1*$^{-/-}$ mice. Significant difference between *Bmal1*$^{fl/fl}$ and *Avp-Cre;Bmal1*$^{wt/fl}$ mice was not detected in any parameters.

SUPPLEMENTAL EXPERIMENTAL PROCEDURES

Generation of *Avp-Bmal1*$^{-/-}$ Mice

For generating *Avp-Cre* mice, we chose a BAC clone (RP23-100C5) from a CHORI BAC library (https://bacpac.chori.org/home.htm), which contains 206 kb genomic DNA derived from C57BL/6J encompassing the *Avp* gene. This BAC was modified using recombineering technology (Lee et al., 2001), to insert a 2.8-kb DNA cassette immediately 5' to the translation initiation codon of *Avp* gene. The DNA cassette contains the ORF of the improved Cre recombinase (iCre) with a nuclear localization signal (provided by Dr. Rolf Sprengel)(Shimshek et al., 2002), followed by the SV40 polyadenylation signal and an kanamycin resistance gene flanked by two FLP sites in the same orientation, which was subsequently removed (Lee et al., 2001). A loxP site in the backbone vector pBACe3.6 was then replaced with a zeomycin resistance gene using *p23loxZeo* plasmid (provided by Dr. Junji Takeda). The circular modified BAC was microinjected into fertilized mouse eggs (C57BL/6J strain) to generate founder lines. Founder animals were mated with C57BL/6J mice (Japan SLC) for characterization and maintenance.

We screened 7 lines for Cre expression by in situ hybridization detecting *iCre* mRNA expression and by crossing to the Cre reporter line *Rosa26R-lacZ* (Soriano, 1999) and selected the line with the best expression in the SCN for further analyses. The specificity of Cre-mediated recombination in the selected line was further examined by mating to another Cre reporter line *Rosa26-tdTomato* mice (Ai14 mice) (The Jackson Laboratory #007914)(Madisen et al., 2010) and immunostaining (see below). To generate *Avp-Bmal1*$^{-/-}$ mice, *Avp-Cre* mice were mated to mice with a conditional *Bmal1* allele (*Bmal1*^{fl}) (Storch et al., 2007) (N>9 backcrossed to C57BL/6J, The Jackson Laboratory #007668).

Mice were maintained under a strict 12-hour light:dark cycle in a temperature- and humidity-controlled room and fed ad libitum. All experimental procedures involving animals were approved by the appropriate institutional animal care and use committees of Kanazawa University, Hokkaido University, and RIKEN BSI.

Behavioral Analyses

Male *Avp-Bmal1*$^{-/-}$ (*Avp-Cre*;*Bmal1*$^{fl/fl}$) and control (*Bmal1*$^{fl/fl}$ and *Avp-Cre*;*Bmal1*$^{wt/fl}$) mice, aged 8 to 25 weeks, were housed individually in a cages placed in a light-tight chamber (light intensity was approximately 50 lux). Spontaneous locomotor activity was monitored by infrared motion sensors (O'Hara) in 1-min bins. Actogram, activity profile, χ^2 periodogram, and FFT analyses were carried out using ClockLab (Actimetrics). The free-running period was measured by periodogram, as well as by FFT and visual inspection, for days 15–29 in DD. The activity period was calculated from the daily activity profile (average pattern of activity) of the same 15 days, using the mean activity level as a threshold for detecting the onset and the offset of activity time (Colwell et al., 2003), or by visual inspection. To determine the light-induced phase shift of locomotor activity, animals in their home cages were exposed to a 30-min pulse of white light (approximately 50 lux) at CT14. The onset and end of nocturnal activity were determined by visual inspection on actograms for measuring light-induced phase shift of activity and the number of days required for reentrainment after abrupt shifts of the LD cycles.

Generation and focal injection of recombinant AAV vectors

The AAV-2 ITR-containing plasmid *pAAV-DIO-hChR2(H134R)-EYFP-WPRE-pA* (provided by Dr. Karl Deisseroth) was modified to construct *pAAV-Bmal1ext-DIO-Bmal1* by replacing *EF1α* promoter and *hChR2(H134R)* cDNA with *Bmal1 ext* promoter (provided by Dr. Isabelle Schmutz)(Schmutz et al., 2010) and Flag-tagged mouse *Bmal1* cDNA (provided by Dr. Kazuhiro Yagita)(Kiyohara et al., 2006), respectively.

Recombinant AAV vectors expressing *Bmal1* or *mCherry* in a Cre-dependent manner were produced using a triple-transfection, helper-free method and purified as described previously with modifications (Lazarus et al., 2011; Sasaki et al., 2011). Briefly, 293A cells (Invitrogen) were transfected with *pHelper* (Stratagene), *pAAV2-rh10* (provided by Penn Vector Core), and either *pAAV-Bmal1ext-DIO-Bmal1* or *pAAV-EF1α-DIO-mCherry* (provided by Dr. Bryan Roth) using a standard calcium phosphate method. Three days later, the transfected cells were collected and suspended

in PBS containing 1 mM $MgCl_2$. After 2 freeze-thaw cycles, the cell lysate was treated with benzonase nuclease (Merck) at 37°C for 30 min, and centrifuged 2 times at 16,000 g for 10 min. The supernatant was used as the virus-containing solution. The titers of recombinant AAV vectors were determined by quantitative PCR: AAV-Bmal1ext-DIO-Bmal1, 1.0 x 10^{13}; AAV-EF1α-DIO-mCherry, 1.0 x 10^{13} genome copies/ml.

We injected the mixture of AAV-Bmal1ext-DIO-Bmal1 and AAV-EF1α-DIO-mCherry (ratio 5:1) into the SCN of two *Avp-Bmal1*$^{-/-}$ and three *Avp-Bmal1*$^{-/-}$*;Per2::Luc* mice so that we could evaluate the efficiency and specificity of expression by immunostaining of mCherry. The stereotaxic injection of AAV vectors was performed as described previously (Sasaki et al., 2011); 1.0 μl of virus solution was delivered to each site (0.1 μl/min). After 5 min of rest, the needles were removed. The stereotaxic coordinates of the Hamilton needle syringe placement for the SCN was: bregma -0.5 mm, lateral ± 0.25 mm, ventral 5.7 mm. One week after surgery, mice started to be monitored for their locomotor activity.

Sleep Recordings

The implantation of an EEG/EMG electrode was performed as described previously (Sasaki et al., 2011). After surgery, all animals were housed individually for a recovery period of at least 14 days. After the recovery period, EEG/EMG recordings were performed on three consecutive days in LD12:12 and then on 11 days in DD. The EEG/EMG data were analyzed as previously described (Sasaki et al., 2011).

Histological Study

To examine the specificity of Cre-mediated recombination, *Avp-Cre*;*Rosa26-tdTomato* mice were pretreated with intracerebroventricular injections of colchicine (40 μg in 1 μl saline). Animals were sacrificed 48 hr later, at approximately ZT8 by transcardial perfusion of PBS followed by 4% paraformaldehyde fixative. To examine the *Bmal1* deletion in *Avp-Bmal1*$^{-/-}$ mice, these mice were further crossed to *Rosa26-tdTomato* mice (Madisen et al., 2010), and the numbers of BMAL1-positive cells were compared between *Avp-Cre*;*Bmal1*$^{fl/fl}$*;Rosa26-tdTomato* and *Avp-Cre*;*Bmal1*$^{wt/fl}$*;Rosa26-tdTomato*

mice (without colchicine pretreatments). Serial coronal brain sections (30 μm thick) were collected in four series, one of which was further immunostained or in situ hybridized. Immunostaining was performed as previously described (Hasegawa et al., 2014; Mieda et al., 2004). The antibodies used were: rabbit anti-AVP (Millipore, 1:4000); rabbit anti-VIP (Immunostar, 1:2000); rabbit anti-BMAL1 (Novus Biologicals, 1:10000); and Alexa 488-conjugated Goat anti-rabbit IgG (Molecular Probes, 1:2000). The expression of tdTomato and mCherry was detected by its native fluorescence or by staining with rabbit anti-DsRed (Clontech, 1:2000), biotinylated anti-rabbit antibody (Vector Labs, 1:500), and the Vectastain ABC kit (Vector Labs) (Figure S1).

A representative optical section was imaged from each stained section by laser-confocal microscopy (Olympus, FluoView FV10i), and fluorescent cells in the images were counted for Figure 1. AVP peptide expression level (Figure S3B) was quantified essentially as described below for quantification of mRNA.

In situ hybridization was performed as previously described (Mieda et al., 2006) using antisense riboprobes labeled with digoxigenin-UTP. Brains were collected at ZT15 with/without 30 min light pulse (for detecting *Per1* induction by light pulse) or at the indicated time on the first day in DD (for measuring circadian expression of *Per1*, *Avp*, *Prok2*, and *Rgs16*). Antisense riboprobes were synthesized from plasmids containing mouse *Per1* (NM_011065, nucleotides 3443-4515)(Mieda et al., 2006), mouse *Avp* (BC051997, nucleotides 337-531), mouse *Prok2* (AF487280, nucleotides 1-528), and mouse *Rgs16* (NM_011267, nucleotides 24-761) cDNAs. mRNA expression levels were quantified by Photoshop (Adobe) as follows. First, the images were transformed to grayscale. Then, mean intensities of pixels within the region of interest were calculated. The values of the region adjacent to the SCN were regarded as background and were subtracted from those of the SCN. For expression analyses of *Per1*, *Avp*, *Prok2*, and *Rgs16*, brains from both male and female mice were used.

Bioluminescence Imaging

Avp-Bmal1$^{-/-}$ mice were further mated with *Per2::Luc* reporter mice (Yoo et al., 2004)(*Avp-Cre;Bmal1*$^{fl/fl}$*;Per2::Luc*) and compared with control mice (*Bmal1*$^{fl/fl}$*;Per2::Luc*). Male and female mice were housed in DD for 3 to 10 weeks

before sampling. PER2::LUC bioluminescence at the SCN tissue level was measured with a photomultiplier tube (Atto, Kronos Dio) at 10-min intervals with an exposure time of 1 min. Coronal SCN slices of 300 μm were made with a vibratome (Leica, Vi1000S). The SCN tissue was dissected at the mid-rostrocaudal region and a paired SCN was cultured on a Millicell-CM culture insert (Millipore) as previously described (Yamazaki and Takahashi, 2005). Recorded values were detrended by subtracting 24-hr moving average values and then were smoothened with a five-point moving average method. Because luminescence from the SCN of *Avp-Bmal1*$^{-/-}$*;Per2::Luc* mice was weak and its waveform was noisy, the middle of the time points crossing value 0 upward and downward were defined as acrophases, and the intervals between two adjacent acrophases were calculated for the periods. Note that very similar results were obtained also when the acrophases were defined as the time points with the maximal values within each cycle.

PER2::LUC bioluminescence at the single SCN cell level was measured with an EMCCD camera (ImagEM, Hamamatsu photonics; iXol, Andor) or a high-sensitive cryogenic CCD camera (ORCA-II ER; Hamamatsu Photonics). Coronal slices of 100 μm were prepared from adult mice with a microslicer (DTK-1000; Dosaka EM) approximately CT8–12 after monitoring locomotor activity in DD for 3 to 10 weeks. The SCN tissue was cultured as previously reported (Ono et al., 2013). Bioluminescence was measured every 60 min with an exposure time of 59 min for 3-5 days. Resolution of images was adjusted to 4.3 μm/pixel, and then data for the individual pixels were detrended and cosine curve-fitted using a custom-made program (Enoki et al., 2012) with minor modifications. Pixels with non-significant Pearson correlation coefficients are shown as black pixels (Figure 7C) and were eliminated for calculating mean and SD of amplitude and period. Amplitudes were relative values within each slice. Pixels with significant oscillation ($p < 0.01$) with period longer than 34 hr were indicated as white pixels in the period maps (Figure 7C) and were eliminated for calculating the mean and SD of the period. The dorsal or ventral SCN were defined as pixels within the dorsal or ventral 40% region for individual unilateral SCNs.

SUPPLEMENTAL REFERENCES

Colwell, C.S., Michel, S., Itri, J., Rodriguez, W., Tam, J., Lelievre, V., Hu, Z., Liu, X., and Waschek, J.A. (2003). Disrupted circadian rhythms in VIP- and PHI-deficient mice. Am J Physiol Regul Integr Comp Physiol *285*, R939-949.

Enoki, R., Kuroda, S., Ono, D., Hasan, M.T., Ueda, T., Honma, S., and Honma, K. (2012). Topological specificity and hierarchical network of the circadian calcium rhythm in the suprachiasmatic nucleus. Proc Natl Acad Sci U S A *109*, 21498-21503.

Kiyohara, Y.B., Tagao, S., Tamanini, F., Morita, A., Sugisawa, Y., Yasuda, M., Yamanaka, I., Ueda, H.R., van der Horst, G.T., Kondo, T., *et al*. (2006). The BMAL1 C terminus regulates the circadian transcription feedback loop. Proc Natl Acad Sci U S A *103*, 10074-10079.

Lazarus, M., Shen, H.Y., Cherasse, Y., Qu, W.M., Huang, Z.L., Bass, C.E., Winsky-Sommerer, R., Semba, K., Fredholm, B.B., Boison, D., *et al*. (2011). Arousal effect of caffeine depends on adenosine A2A receptors in the shell of the nucleus accumbens. J Neurosci *31*, 10067-10075.

Lee, E.C., Yu, D., Martinez de Velasco, J., Tessarollo, L., Swing, D.A., Court, D.L., Jenkins, N.A., and Copeland, N.G. (2001). A highly efficient Escherichia coli-based chromosome engineering system adapted for recombinogenic targeting and subcloning of BAC DNA. Genomics *73*, 56-65.

Mieda, M., Williams, S.C., Sinton, C.M., Richardson, J.A., Sakurai, T., and Yanagisawa, M. (2004). Orexin neurons function in an efferent pathway of a food-entrainable circadian oscillator in eliciting food-anticipatory activity and wakefulness. J Neurosci *24*, 10493-10501.

Ono, D., Honma, S., and Honma, K. (2013). Cryptochromes are critical for the development of coherent circadian rhythms in the mouse suprachiasmatic nucleus. Nat Commun *4*, 1666.

Sasaki, K., Suzuki, M., Mieda, M., Tsujino, N., Roth, B., and Sakurai, T. (2011). Pharmacogenetic modulation of orexin neurons alters sleep/wakefulness states in mice. PLoS One *6*, e20360.

Schmutz, I., Ripperger, J.A., Baeriswyl-Aebischer, S., and Albrecht, U. (2010). The mammalian clock component PERIOD2 coordinates circadian output by interaction with nuclear receptors. Genes Dev *24*, 345-357.

Soriano, P. (1999). Generalized lacZ expression with the ROSA26 Cre reporter strain. Nat Genet *21*, 70-71.

Yamazaki, S., and Takahashi, J.S. (2005). Real-time luminescence reporting of circadian gene expression in mammals. Methods Enzymol *393*, 288-301.